UNIVERSITY OF WEST BOHEMIA

FACULTY OF MECHANICAL ENGINEERING

Study programme: N0715A270011 – Machining, Additive Technology, and quality assurance

Study specialization: None

DIPLOMA THESIS

Investigation of SLM process Phenomena by means of In Situ Monitoring Systems

Author: Bc. Yusuf BAKIR

Supervisor: Ing. Ivana ZETKOVÁ, Ph.D.

Academic Year 2021/2022

ZÁPADOČESKÁ UNIVERZITA V PLZNI
Fakulta strojní
Akademický rok: 2021/2022

ZADÁNÍ DIPLOMOVÉ PRÁCE

(projektu, uměleckého díla, uměleckého výkonu)

Jméno a příjmení:	**Bc. Yusuf BAKIR**
Osobní číslo:	**S19N0097P**
Studijní program:	**N0715A270011 Obrábění, aditivní technologie a zabezpečování kvality**
Téma práce:	**Investigation of SLM process Phenomena by means of In Situ Monitoring Systems**
Zadávající katedra:	**Katedra technologie obrábění**

Zásady pro vypracování

1. Introduction
2. Analysis of the current state
3. Proposal for design and realization of my experiments
4. Evaluation of results and recommendations
5. Conclusion

Rozsah diplomové práce:	**50 – 70 stran**
Rozsah grafických prací:	**dle potřeby**
Forma zpracování diplomové práce:	**tištěná/elektronická**
Jazyk zpracování:	**Angličtina**

Seznam doporučené literatury:

- GIBSON, Ian, ROSEN, David a STUCKER, Brent. Additive manufacturing technologies: 3D printing, rapid prototyping, and direct digital manufacturing. Second edition. New York: Springer, [2015], 2015. xxi, 498 stran. ISBN 978-1-4939-2112-6.
- GEBHARDT, Andreas. Understanding additive manufacturing: rapid prototyping, rapid tooling, rapid manufacturing. Munich: Hanser, [2012], 2011. ix, 164 stran. ISBN 978-3446425521.
- DIEGEL, Olaf, NORDIN, Axel a MOTTE, Damien. A practical guide to design for additive manufacturing. Singapore: Springer, [2020], 2020. xx, 226 stran. Springer series in advanced manufacturing. ISBN 978-981-13-8280-2.

Vedoucí diplomové práce:	**Ing. Ivana Zetková, Ph.D.** Katedra technologie obrábění
Konzultant diplomové práce:	**Doc. Ing. Miroslav Zetek, Ph.D.** Regionální technologický institut
Datum zadání diplomové práce:	**15. října 2021**
Termín odevzdání diplomové práce:	**27. května 2022**

L.S.

Doc. Ing. Milan Edl, Ph.D. děkan	**Doc. Ing. Jan Řehoř, Ph.D.** vedoucí katedry

Prohlášení o autorství

Předkládám tímto k posouzení a obhajobě diplomovou práci, zpracovanou na závěr studia na Fakultě strojní Západočeské univerzity v Plzni.

Prohlašuji, že jsem tuto diplomovou práci vypracoval samostatně, s použitím odborné literatury a pramenů, uvedených v seznamu, který je součástí této diplomové práce.

V Plzni dne: ……. …….

podpis autora

Gratitudes

Firstly, I would like to thank my supervisor Ing. Ivana Zetková, Ph.D., for professional guidance and support throughout this work from the idea phase to execution. I would also like to thank the head of our laboratory doc. Ing. Miroslav Zetek, Ph.D. for enabling me to carry out the experiments and evaluations that were necessary for this work. Special thanks to my colleague Ing. Martin Bureš for his continuous help all along the making of this work. Last but not least, I am grateful to my family for their endless support during my studies and the help during this work.

ANOTAČNÍ LIST DIPLOMOVÉ PRÁCE

AUTOR	**Příjmení** BAKIR	**Jméno** Yusuf	
STUDIJNÍ PROGRAM	N0715A270011 Obrábění, aditivní technologie a zabezpečování kvality		
VEDOUCÍ PRÁCE	**Příjmení (včetně titulů)** Ing. Zetková, Ph.D.	**Jméno** Ivana	
PRACOVIŠTĚ	ZČU - FST - KTO		
DRUH PRÁCE	**DIPLOMOVÁ**	~~**BAKALÁŘSKÁ**~~	**Nehodící se škrtněte**
NÁZEV PRÁCE	Zkoumání procesních jevů SLM pomocí in situ monitorovacích systémů		

FAKULTA	strojní		**KATEDRA**	KTO	**ROK ODEVZD.**	2022

POČET STRAN (A4 a ekvivalentů A4)

CELKEM	68		**TEXTOVÁ ČÁST**	57	**GRAFICKÁ ČÁST**	0

STRUČNÝ POPIS (MAX 10 ŘÁDEK) **ZAMĚŘENÍ, TÉMA, CÍL POZNATKY A PŘÍNOSY**	Obecným cílem této práce je pozorovat a prozkoumat některé jevy, které probíhají během procesu selektivního laserového tavení. Proces SLM je velmi komplexní a jeho předností je velká svoboda konstrukčních návrhů vyráběných geometrií. Pro lepší vysvětlení fungování tohoto procesu je v práci použit monitorovací systém využívající optické tomografie a pomocí něho je testováno několik strategií s ohledem na mechanické vlastnosti a data z monitorovacího systému.
KLÍČOVÁ SLOVA **ZPRAVIDLA JEDNOSLOVNÉ POJMY, KTERÉ VYSTIHUJÍ PODSTATU PRÁCE**	Selektivní Laserové Tavení, Mechanické vlastnosti, In Situ monitorování, Vyhodnocování dat

SUMMARY OF DIPLOMA SHEET

AUTHOR	**Surname** BAKIR	**Name** Yusuf
STUDY PROGRAMME	N0715A270011 Machining, Additive Technology, and quality assurance	
SUPERVISOR	**Surname (Inclusive of Degrees)** Ing. Zetková, Ph.D.	**Name** Ivana
INSTITUTION	ZČU - FST - KKS	

TYPE OF WORK	**DIPLOMA**	**~~BACHELOR~~**	**Delete when not applicable**
TITLE OF THE WORK	Investigation of SLM process Phenomena by means of In Situ Monitoring Systems		

FACULTY	Mechanical Engineering		**DEPARTMENT**	KTO		**SUBMITTED IN**	2022

NUMBER OF PAGES (A4 and eq. A4)

TOTALLY	68		**TEXT PART**	57		**GRAPHICAL PART**	0

BRIEF DESCRIPTION **TOPIC, GOAL, RESULTS AND CONTRIBUTIONS**	General scope of this work was to observe and investigate some of the phenomena that are taking place during Selective Laser Melting process. The SLM process is very complicated and its premise is near limitless geometrical freedom during manufacturing. In order to better explain the workings of this process Optical Tomography monitoring system was utilized. And several strategies were tested with respect to mechanical properties and monitoring data.
KEY WORDS	Selective Laser Melting, Mechanical Property, In Situ Monitoring, Data Evaluation

Content

List of Abbreviations

AM	Additive Manufacturing
CAD	Computer-Aided Design
SLM	Selective Laser Melting
EBM	Electron Beam Melting
OT	Optical Tomography
CMOS	Complementary Metal Oxide Semiconductor
CCD	Charged Coupled Device
SLI	Spectral Library Format
SLC	SLiCe Format File
CLI	Common Layer Interface
SEM	Scanning Electron Microscopy
VED	Volumetric Energy Density
TGM	Temperature Gradient Mechanism
CT	Computed Tomography
MPM	Melt pool Monitoring
GV	Grey Value
HV10	Vickers hardness test with the load of 10 Kg

List of Units

P	[W]	Laser Power
v	[mm/s]	Scanning Speed
h	[mm]	Hatch Spacing
t	[mm]	Layer Thickness
E	[J/mm^3]	Volume Energy Density
$R_{p0.2}$	[Mpa]	Offset Yield Strength
R_m	[Mpa]	Tensile Strength

List of Figures

List of Tables

1 Introduction

Additive Manufacturing (AM) is a relatively new field of production with a new approach to the manufacturing industry. This term includes many different types of processes. In general, as opposed to conventional means of manufacturing, AM is creating a part based on 3D CAD data by joining layers of materials one after another. It emerged as a way to create prototypes and this technology was used under the name of rapid prototyping until the 21st century. Thanks to improvements the technology and a decrease in operating costs, in last the two decades additive manufacturing has evolved into a feasible means of production for repeatedly produced parts as well.

Selective Laser Melting (SLM) is one of many types of AM. It is, with regards to stock material, a powder-based process with a building platform covered with powder with the help of recoating mechanism. Later on, the metal powder is melted and fused by a laser beam in particular areas for each layer and these processes take place repeatedly layer after layer. Possibilities of shapes that can be created by SLM are near-infinite and regardless of the part that is printed raw material is always metal powder. These key characteristics are the main causes for SLM's ability to change production processes substantially. The supply of only one material is sufficient for the process to create near-net-shaped parts. This way supply chain for the production becomes significantly short. Near-to-infinite geometries that can be built, enable the production of complex parts. Due to the same ability, it requires less post-processing and assemblies of the parts can be printed at once. Therefore, production lines are much shorter in comparison to conventional manufacturing methods while almost any required part in a plant can be produced locally.

The SLM process, like every other means of production, has its advantages and disadvantages. For this work, SLM technology employs a laser that has a focus diameter of approximately 100 µm. The focus diameter highly dictates the melt-pool size created during the process. In comparison to other powder-bed AM processes, such as Electron Beam Melting (EBM) which employs an electron beam with a focus diameter of around 350 µm. The SLM is capable of creating more complex geometries however with a lower production rate due to its mechanism that generates relatively more localized melting of metal powder. The interaction time of the laser with the powder and the layers which are printed previously is very short that leads to high cooling rates and thus very fine microstructure. However, owing to the very short time window of interaction with laser and very rapid solidification, the melt-pool created may be unstable. Sudden changes in the solubility of the materials within the melt-pool, may cause quasi-crystalline phases to form, metal vapor may be trapped, and also some particles of the powder may not be successfully melted. SLM builds parts in one direction and repeated heating and cooling cycles during production results in columnar grain structure along the build direction. Therefore, parts possess anisotropy in their mechanical properties based on the axes on which they are printed.

SLM process is in its early stages of development and there are as many as 50 potential factors affecting the quality of the final product of the process. Even though, it is unlikely to control all these factors and phenomena that occur during the SLM process, a careful selection of main process parameters such as laser power, scanning speed, hatch-spacing, and layer thickness may ensure the building of a part to a certain extent. Therefore, thorough inspection and assurance of the quality of the parts that are built by SLM are crucial. Monitoring systems can play a major role in assure sufficient quality that will promote the wide adaptation of printed parts in the

manufacturing industry. As an experimental approach, a testing of the parts after they are built and also a monitoring of them during the SLM processes by in-situ monitoring systems, provide information for the development of the technology. The monitoring systems have the potential to provide insights into the phenomena during the SLM process as well as can point out potential defects within the parts. Thus, becoming and powerful tool for the development of the process.

1.1 Aim of the work

The main goal of this work is to investigate the SLM process by using Optical Tomography(OT) of EOSTATE in-situ monitoring systems as well as, a tensile and a fatigue testing and a metallographic inspection to identify some of the defects that are repeatedly formed during SLM and test the remedies for some problems using modifications of scanning strategy of the laser.

The first problem to be tackled by this work will be the distraction of laser energy due to residual particles- side products of creating a melting pool. During the melting phase, due to the high energy of the laser and fluidity of the metal powder, clusters of metal vapor, spattering particles, and plasma are formed. Some of the formed particles ascend above the melt pool and create a cloud. The cloud of materials, if intersected with the laser beam, might cause unexpected results as instead of localized laser irradiation and melting, de-focusing the laser beam might create uneven melting of multiple locations on the powder bed. The solution that will be proposed for this problem will be to adjust the scanning strategy in a way to utilize inert gas flow in the building chamber of the SLM machine to transport the cloud out of the way of the laser beam.

The second problem that will be worked on is related to the thermal mapping of relatively thin parts are prone to deformation while being printed. Due to the shrinkage of the molten material while solidification, thermal stresses are generated. A part's geometry highly dictates the timeframe in which the heat input is given to a material, and at the same time it also effects the ability of the part to resist thermal stresses. For this problem, scanning strategies that target more uniform heat input throughout all layers of a part, will be employed.

Eostate Exposure monitoring systems provide important data for tracking these problems. Optical Tomography system utilizes a CMOS industrial camera to record and to create a map based on irradiation from the melt pool. At the same time, the Melt-pool monitoring system exploits photodiodes to observe melt pool dynamics. In addition to these two systems, The Powderbed monitoring system is used for checking the recoating process of each layer. In this work, data recorded by Eostate monitoring systems will be used as a reference point for finding the root cause of the error with the parts. Solutions will be suggested the and overall effects of solutions on mechanical and metallographic properties of the parts will be evaluated to examine the validity of the solutions.

2 Analysis of the current state

2.1 Introduction to SLM technology

This subchapter will be about general explanations of basic concepts of the SLM process. Although, the SLM process is similar to welding, as it works by melting and combining parts by a source of heat, the manner in which the welding takes place is radically different. The SLM consists of numerous, selectively localized welding processes in shorter time windows.

Therefore, this technology has its unique mechanisms during the production of a part which enables the process to build parts for complex geometries as can be seen in Figure 1.

Figure 1 Components built by SLM for automotive and aerospace industries.[1]

Fundamental mechanisms of SLM which have the main effects on the building of a part will be explained in the following chapters as well as the errors that are formed will be explained.

2.1.1 Working principles of SLM

There are a few steps of modification and necessary transformation of any data to be used in an SLM machine. For a CAD file to be printable by the SLM process, a part must be oriented on the building platform of the SLM machine, support structures for the down-facing surfaces must be generated and the previously CAD file is saved as SLI, SLC, or CLI file which contains the data for the parts and support structures, these modifications are carried by specific softwares such as Magics RP by Materialise, Viscam by Marcam, and Netfabb by FIT.[2]

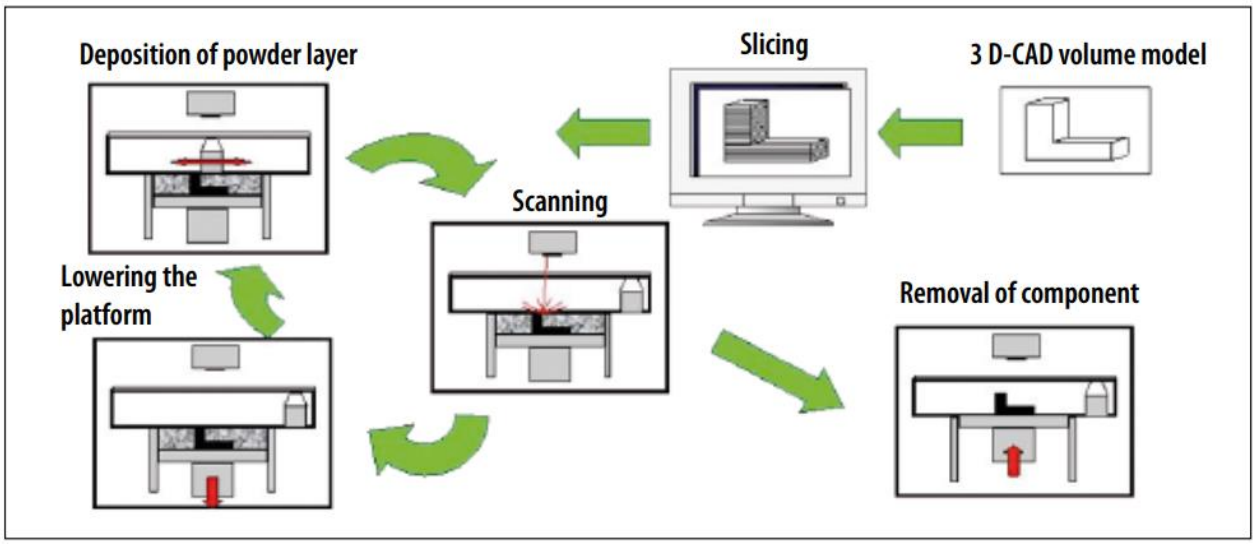

Figure 2 Data preparation and production steps by SLM.[3]

In Figure 2 data preparation is named Slicing. Material properties, aim of the printing process, and machine specifications are considered during Slicing and necessary data for scanning each layer is prepared. After this process is carried out, data is sent to SLM machine. The building

process begins with covering the building platform with metal powder. The thickness of this raw powder layer is dictated by lowering the building platform as it creates the gap between the recoater and the building platform, which later will be filled by powder. Subsequently, specific areas of the layer which should contain the solid part are scanned by laser.

Recoating and scanning is repeated for each layer until parts are built.[3] Due to high temperatures reached during SLM process the risk of oxidation is very high. Thus, the production by this process takes place under inert gas atmosphere. Oxygen content should be lower than 0.3 %.[4] Argon and nitrogen are used to provide protective environment while they might affect the microstructure of the particles as well as microstructure of parts. Therefore, suitable inert gas should be selected based on material being used for production.[5]

For every AM process the slicing step is different and requires different data preparation due to the mechanisms of that particular production technique. Figure 3, demonstrates the possible orientations for a part and the results of each orientation in terms of manufacturability, laser scanned area per layer, surface roughness, areas to be supported and so on. Therefore, selecting building orientation becomes an optimization problem that should be solved while taking into consideration multiple criteria and process mechanisms.

Another phenomenon that can be seen in the figure is the application of support structures. Part orientation determines the course of the print to a certain degree which means some of the main mechanisms that take place during a print are pre-calculated and orientation is based on solving the potential problems. During a print part is subjected to thermal cycles and phase changes thus resulting in stresses within the part, in addition to those forces are applied on the part during recoating process due to the friction between the powder particles as well as possible contact between the part and recoater blade. Supports structures are used to compensate for the shot-comings of selected orientation. The function of these structures can be counter-balancing thermal stresses within the part, increasing the heat conduction as well as increasing the stiffness of the built against the forces created by recoating.[6]

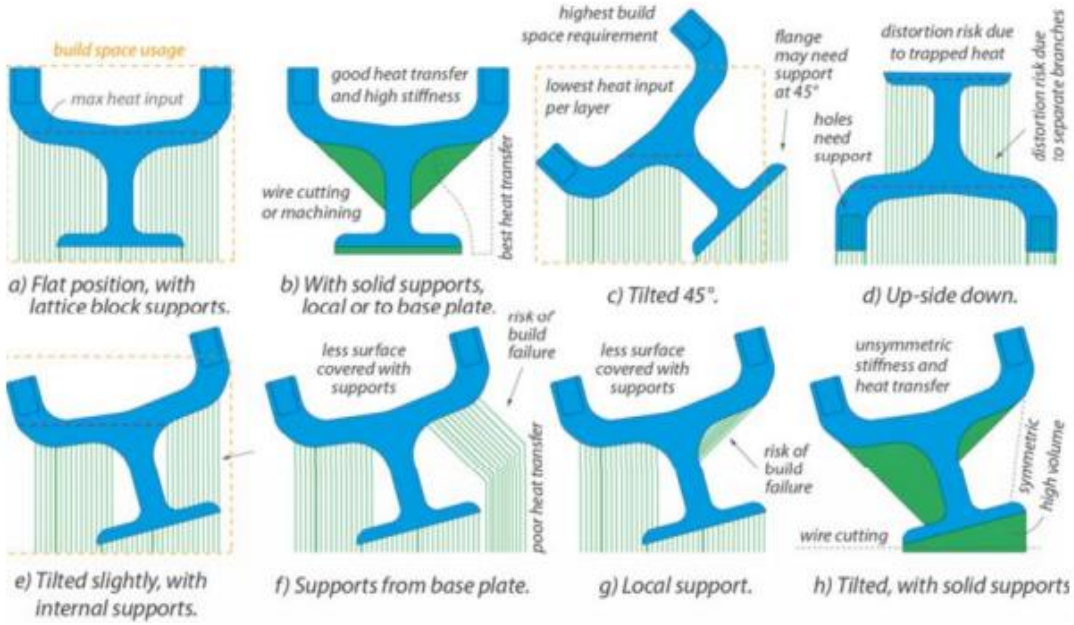

Figure 3 Support designs for different part orientations.[6]

2.1.2 Materials used for SLM

The form of the raw materials that are being used for SLM is fine powder as pointed out before. Materials used, need to meet the special requirements of both scanning and recoating processes of the SLM process as well as have the mechanical properties necessary for utilization of parts that are built.

Steel alloys are commonly used in the industry thanks to their high hardness, high strength, and corrosion resistance. However, some other mechanical properties of materials also affect the effectiveness of the process. An example of this phenomenon can be the printing of Tin-bronze parts. While this material demonstrates high wear resistance and high thermal conductivity, it also has a very low laser absorption rate. As a result scanning of this metal requires high laser power and low scanning speed to obtain sufficient density. [1]

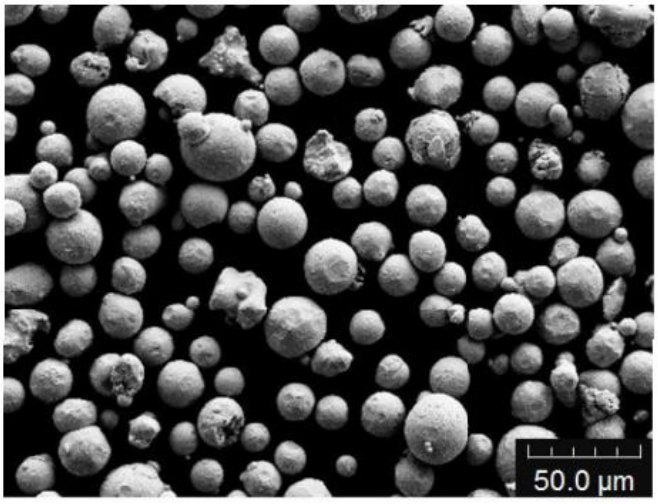

Figure 4 SEM image of powder raw loose powder.[7]

Another aspect of the material used is the particle size of the powder and its variability. The Figure 4, the result a of Scanning electron microscopy(SEM) of analysis result of maraging steel 300 is given. According to this result, the size range of powder globes varies between 5.67 and 33.88 µm in diameter. According to sieving analysis according to ASTMB214, EOS Maraging Steel MS1 powder that is used on this work has maximum particle diameter of 63 µm which is ensured by the sieving filter's mesh size.

Packing density of the powder is crucial for obtaining high density and lower surface roughness on the parts. While fine particles provide bigger surface area for the laser absorption during scanning, wider distribution of the particle sizes generates higher density due to the fact that particles are in the shape of globes; smaller globes filling in the gaps created between the particles with bigger diameters. In addition to those, bigger size of particles may cause problems during recoating by being stuck under recoating blade and being dragged throughout building platform along recoating direction.[8]

2.1.3 Process Parameters

For SLM parts to perform as expected under working conditions, high energy density is required. And careful selection of process parameters for a printing job is crucial to obtain the high density with minimized potential of errors during the job. Main process parameters of SLM process are as mentioned before; laser power, scanning speed, hatch spacing and layer thickness.

There have been numerous works carried out, investigating the effect of process parameters on the relative density of the parts, in the literature. Improper selection of these parameters leads to porous parts that do not have the suitable mechanical properties that are required. Therefore, equations suggested and tested in order to investigate the relation of process parameters to the relative density of the parts.

$$E\left(\frac{J}{mm^3}\right) = \frac{P(W)}{v\left(\frac{mm}{s}\right).h(mm).t(mm)} \tag{2.1}$$

The formula given here commonly named as Volumetric Energy Density(VED) is one of the approaches aiming to develop process parameters for SLM process. Laser power(P), Scanning speed(v), hatch spacing(h) and layer thickness(t) are being used.[7] Here, the ratio of power provided by the laser to the volume of the powder that is being melted is calculated. The amount of the energy given should be large enough for powder to completely melt and result in epitaxial solidification in order to obtain highly dense parts.[9] Other variations to VED approach have also been tested in the literature. (Souza et al., 2019) suggested considering the laser spot size while calculating energy intensity instead of hatch spacing, due to laser spot size dictating the area of which laser power is being applied.[8]

The term scanning strategy is used to describe the precise and detailed application of heat energy to powder bed. The utility in using scanning strategies various as such techniques greatly manipulate the amount and direction of the application of the energy given to metal powder. Energy applied per unit time and per unit volume of the powder directly affect the melt-pool formation and deformations within the parts therefore repeatability of the process.

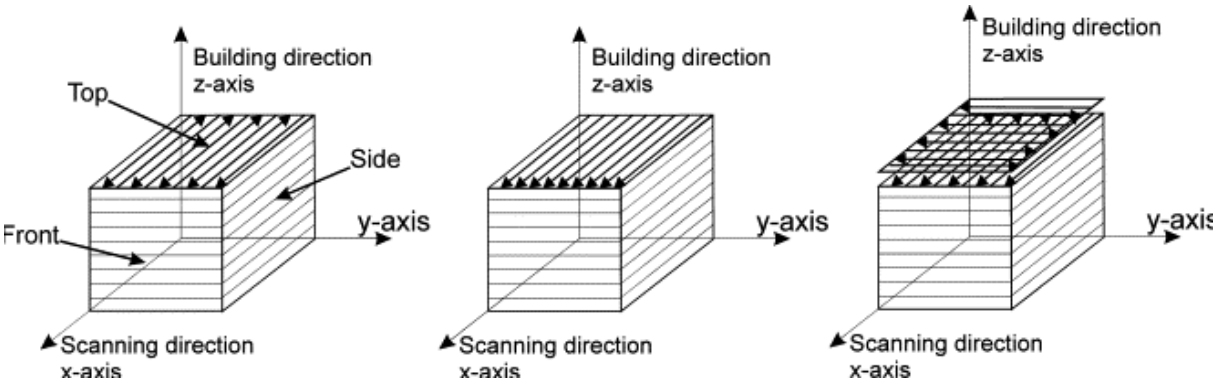

Figure 5 Different scanning strategies, such as zigzag, unidirectional, zigzag and cross hatching.[10]

In Figure 5, simple scanning lines by the laser are shown with arrows. These arrows are usually named as hatching vectors. Hatching vectors dictate the direction of the formation of melt pool. Since during SLM, the energy intensity transferred to the powder bed is high enough to melt

the previously melted layers, elongated grains are formed between subsequent layers. However, such melting modes also mean that if there are any flaws within the previously melted layer, such flaws can grow in built direction. Therefore, scanning strategies can affect the density, microstructure and mechanical properties of parts.[11]

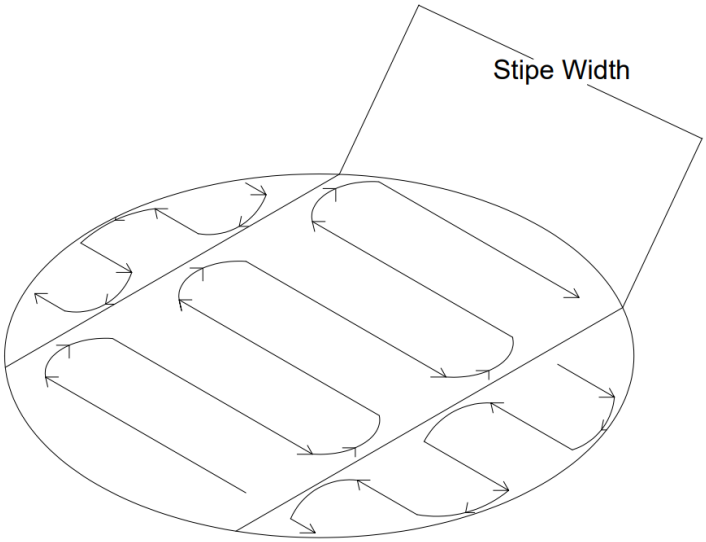

Figure 6 Basic scheme of the stripes scanning strategy.

An example scheme of scanning strategy of laser is given here at the Figure 6. The name of this strategy is called stripes exposure pattern as areas are scanned in the shape of stripes which are filled with hatching movement of the laser. The direction of the stripes is switched with each stripe as it can be seen in the figure while the axis remains the same for all stripes during exposure of a layer. Hatch lines are perpendicular to the stripe axis and hatch length depends on the stripe width, geometry of the scanned layer and overlapping rate of stripes. In addition to the previously shown scanning strategies, with stripes strategy energy is applied to powder bed by shaping islands of stripes in each layer. In order to avoid the flaws elongating throughout multiple layers, the scheme of the strategy is rotated and shifted for each layer.

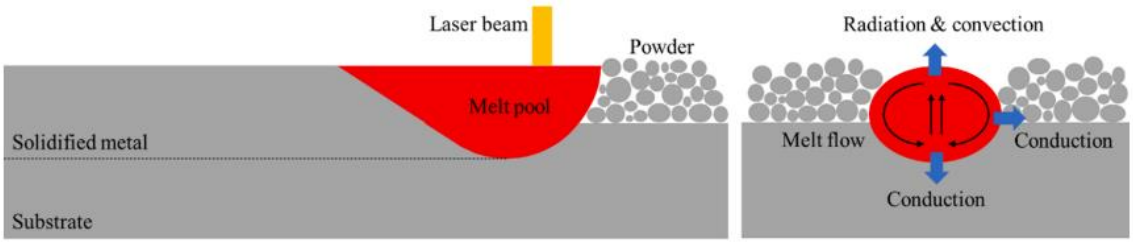

Figure 7 Schematics of laser and powder interaction and heat transfer modes such as conduction, radiation, and convection.[10]

During laser exposure, the heat applied to the loose powder creates melt pool that results in solidified metal. However, as it can be seen in the Figure 7, the heat energy is not fully absorbed by the loose powder while some of it leads to phase transformations, some portion of the heat

is conducted to the substrate and to the loose powder particles around the melt pool. In addition, through radiation and convection some of the heat is given to the environment.

There are two modes of melting during laser welding, which are conduction and keyhole melting. The goal of selecting the optimal process parameters in order to produce high density part is achieved through controlling of the melting modes.

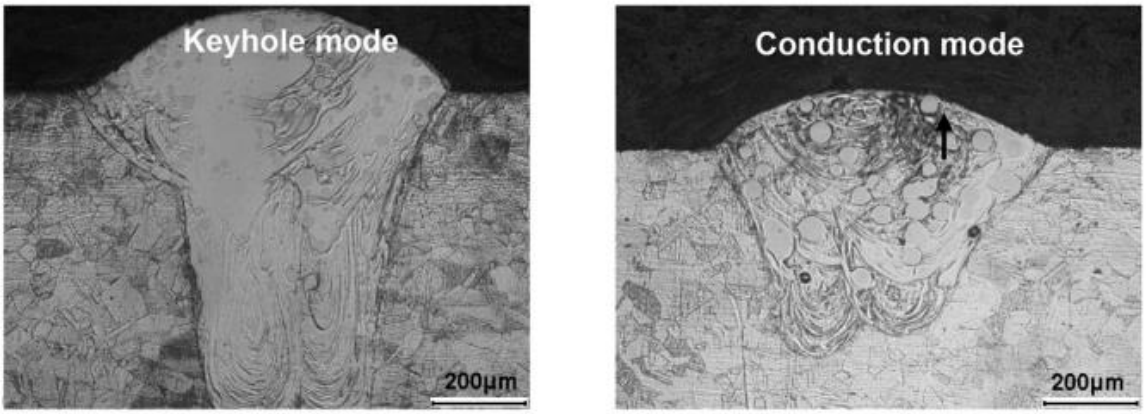

Figure 8 Light microscope images of melting modes during SLM.[12]

Formation of the melting modes are demonstrated in the Figure 8. The transition between the melting modes can be designated by the aspect ratio of the melt pool. For the keyhole melting, the ratio of the width of the melt pool to its depth should be less than 0.5. Keyhole mode results in higher productivity due to its melt pool depth. And, during keyhole melting the conduction rate to the substrate is higher thus resulting in higher cooling rates and finer grain structure. Samples produced under keyhole conditions demonstrate higher strength and ductility. [13]

Threshold between conduction melting and keyhole melting can be used as reference for optimizing the SLM process in terms of the heat input the materials are subjected to. Getting either far below or far above the heat input necessary for transition in between melting modes can result in flaws within the parts.[14]

Due to its manufacturing process characteristics such as high thermal gradients, high thermal solidification rates, layer-wise powder deposition, planar movement of the heat source and building in uniaxial direction, building parts via SLM that demonstrate inherent anisotropy. [8]

2.1.4 Defect formation and Thermal Phenomena During SLM

As mentioned before there are many factors and process settings that affect the quality of the production with SLM technique. Besides process parameters being one of the main settings, other factors such as the density of the powder bed, laser wavelength, 3D geometry of the material, absorptivity and conductivity of the powder etc. It is suggested there are over fifty factors affecting the quality.[4]

In order to demonstrate the complexity of a SLM process, pre-heating the process chamber can be given as an example. Pre-heating can be between 25◦C to 250◦C. Advantages of the pre-heating as it narrows the thermal gradient in the process chamber, the necessary enthalpy for melting becomes lower, thus thermal stresses are decreased as well. However, changing the pre-

conduction heating temperature can also change the absorptivity and conductivity of the material. In conclusion it can be difficult to isolate the effect each parameter have on the process conditions.[4]

With this work combined product of defect formation and thermal phenomena that take place during SLM process will be investigated. Therefore, in this chapter, some of the mechanisms of the process which are directly controlled by the main processing parameters will be explained.

2.1.4.1 Internal Defect formation within SLM production

In this sub-chapter some of the internal flaws of the parts built by SLM production technique and process dynamics that are causing them will be explained. While such defect may cause significant adverse effects on the mechanical properties of the parts built, they also have the potential for leading to errors that would hinder or stop production.

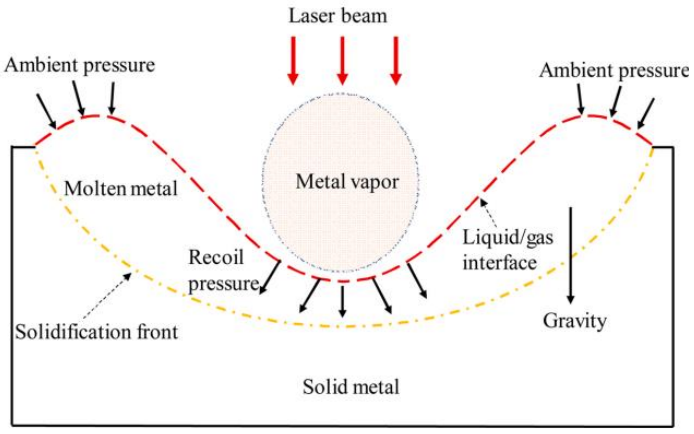

Figure 9 Forces to create and maintain keyhole melting mode.[15]

Figure 9 shows the mechanical forces during keyhole melting. Maintaining the melt pool depth at a certain range is crucial for the SLM process. During the melting of the powder, the evaporated material particles create metal vapor which leads to recoil pressure due to rapid expansion of the gas volume. The depth of the melt pool decreases with the increase ambient temperature. investigates the forces formed around the melt pool while printing with the stainless steel 316L. Moreover, when ambient pressure is over 10^3 Pa (approximately over 1 atm) the metal vapor that is generated and ascended over melt pool decaying the power of the laser. Thus, recoil pressure that keeps the keyhole open is also affected by the ambient pressure. In conclusion, there should be a balance between the forces within the melt pool and with ambient pressure as well as with laser radiation in order to obtain and maintain keyhole melting.[15]

Melt pool overheating and losing the mentioned balance is a common problem during SLM. Locally increased heat input can occur due to scanner dynamics, laser instability and other phenomena. Increasing the laser power locally can lead to higher metal evaporation and turbulences within melt pool. Such instabilities may result in spherical gas pores that are entrapped within the melted material.[16] In addition to that mechanism of spherical pore forming,[17] claims that most of spherical pore formation during SLM is due to the argon gas

bubbles within powder feed stock that are expanding during the process because of lower pressure in building chamber.

Since these kinds of flaws are formed during the melting and the liquids exert pressure in all directions, thus such errors are recognized by their spherical shape as it can be seen in the Figure 10.

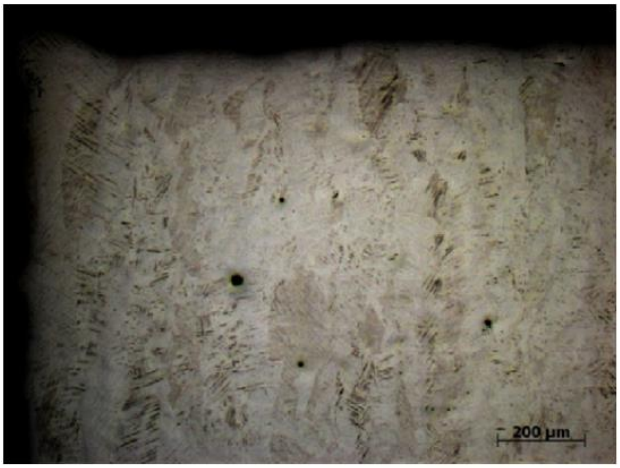

Figure 10 Circular gas entrapment defects.[11]

Another phenomenon that leads to internal pores is lack of fusion(LOF). LOF pores are usually small cavities within the parts that are formed due to unoptimized process parameters. As the name implies such errors are left behind melt pool and they result in unfused metal powder stuck within the parts. LOF defects usually have random geometries (Figure 11). Such internal flaws while affecting the material properties of the parts, can also hinder the solution treatment process of the material MS1, due to their ability to restrain the movement of the grain boundaries.[16]

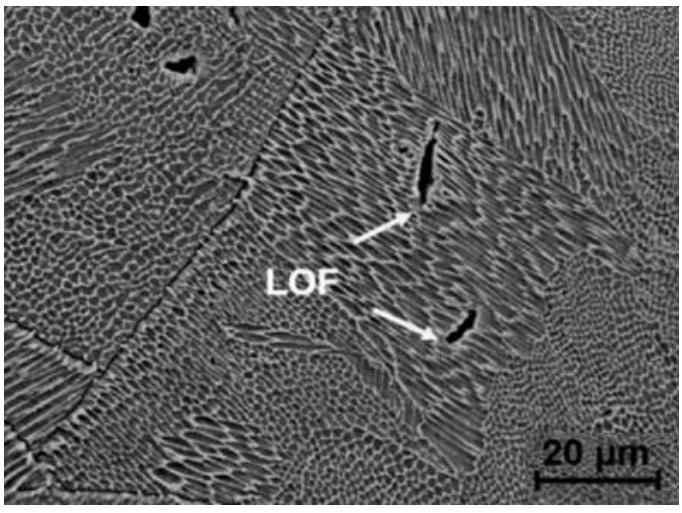

Figure 11 Irregular shaped lack of fusion defects.[16]

Selecting optimum process parameters has proven be vital for producing high quality SLM production in scientific literature. Powder layer denudation and balling are another result of

process parameters and dynamics such as non-uniform heat input and conduction throughout a print job. Both of these mechanisms may lead to LOF pores.

Balling takes place in the form of unstable droplets of melted material instead of smooth continuous melting pool. This mechanism is called Rayleigh instability that leads to break up of fluid thread. [6] Balling may lead to pores of un-melted powder as well as semi-melted powder around the melt-pool. In addition, rough surfaces obtained due to balling may require post-process polishing. In more extreme cases of surface roughness it may also lead to a halt of recoating process thus stopping the building process.[18]

Oxygen content within the metal powder may also increase the balling effect. When the trapped oxygen within the powder is irradiated by the laser, oxygen may lead to higher temperatures within the melt pool therefore higher fluidity. Higher fluidity, increases the chances of melt pool separating into droplets.[19]

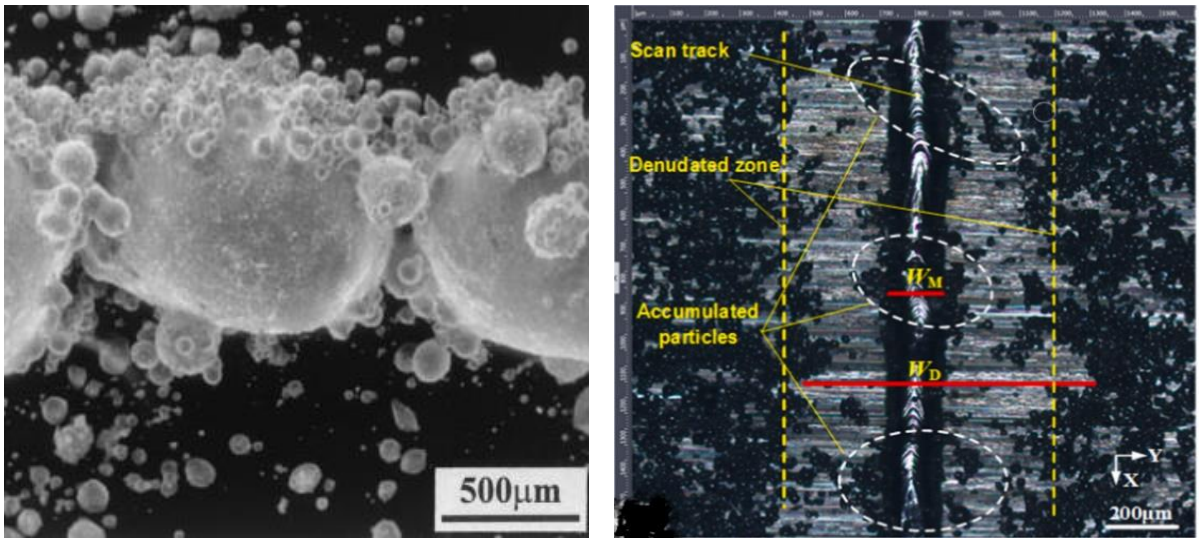

Figure 12 Semi-melted ‘‘satellite‘‘ powder particles and denudation zones around melting tracks.[20]

On the other hand, powder denudation may take place with every process parameter set that is selected. Laser spot size for SLM process is very fine, however during the melting the heat-effected zone of the powder layer may become much bigger than the spot size. Melt pool width is bigger than the diameter of the spot size due to high energy intensity. In addition to that, powder that is laid around the melt pool does not stay still and it may move or splash. Some of the cold particles may be pulled into the tail of the melt pool and get melted or semi melted, thus resulting in LOF pores or satellite particles(Figure 12).[20]

2.1.4.2 Spatter Formation and Gas flow inside the building chamber

In the previous subchapter, the defects that are formed during melting due to the melt pool dynamics were explained. While spatter formation takes place according to the similar phenomena within melt pool, in the spatter formation the material prone to cause defects is ejected from the melt pool. The high amount of heat during melting is also causing the evaporation of the metal material. Evaporation leads to immediate increase in the volume of the material that will cause the recoil pressure as explained before. Recoil pressure is one of the important factors affecting the melting mechanics during SLM as it plays a big role in

maintaining melting modes. In addition, the that recoil pressure is also the main reason behind some of the molten material being ejected from the melt pool.[21]

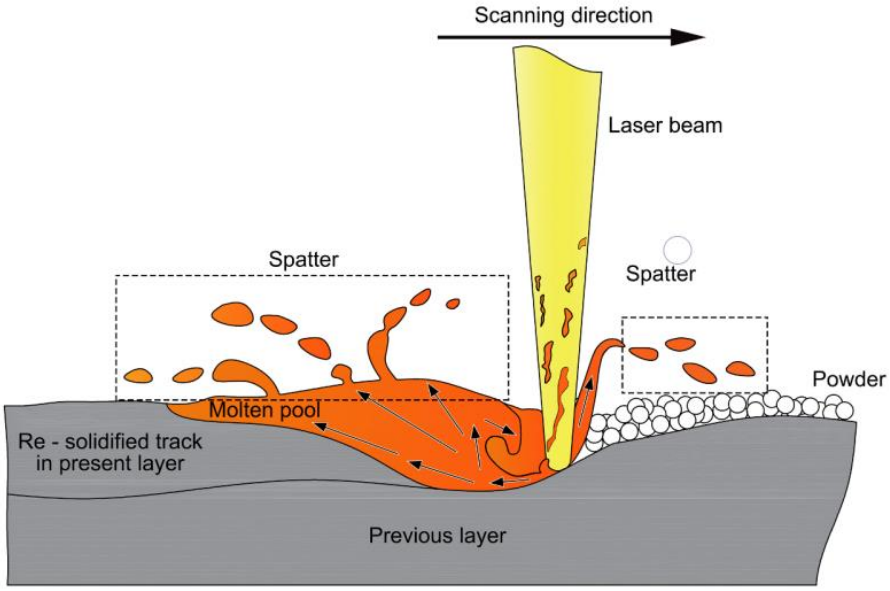

Figure 13 Formation of spatters ejected from melt pool.[21]

Figure 13 demonstrates the formation of spatters. In addition to the spatters being ejected from the melt pool as a result of recoil pressure, yet the mechanism causing the spatters at the back of melt pool is different. The black arrows marking the movement of molten material represent Marangoni effect. Molten material moves from the high temperature zone under the irradiation of the laser to the lower temperature zone at the tail of the melt pool. Here, the recoil pressure causes the molten material with relatively lower viscosity to be ejected. Similarly, to the balling affect, the ejected material also have the tendency to shrink into shape of globes.[21]

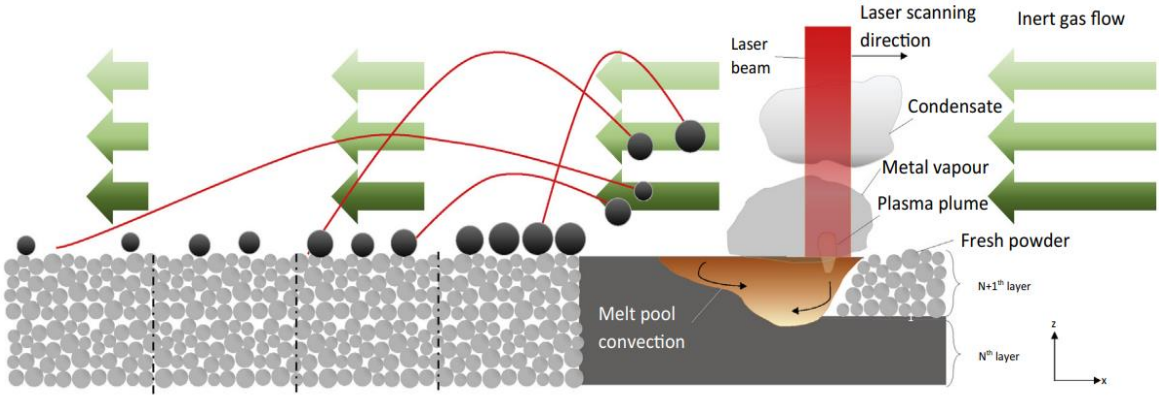

Figure 14 Laser and melt pool side products interaction with respect to gas flow direction.[22]

The complexity of the SLM process has already been mentioned before. Thus, spatter formation is also a phenomenon of which effects cannot be isolated from the general process dynamics. In the Figure 14, the interaction between the spatters ejected and the inert gas flow within the building chamber is given. Transport of the said particles via inert gas has significant affects

both during the process and after the process. Since spatters have already undergone heating and melting process the morphology, size and chemical content can significantly be changed. Thus, contamination of the powder feed stock with spatters can cause problems during both recoating and exposure steps.[22]

Contamination of the powder feed stock can lead to problems while printing multiple parts in the same building chamber as the unused powders around the parts depending to the distance from the parts built, as illustrated in Figure 14. In addition, since the powder is most likely to be used again such contamination may also affect the quality of the subsequent builds. According to (Spatter-mechanical-property-monitoring), while printing with the CoCrW alloy, both carbon and oxygen content within spatters was increased by at least 100%. Oxidation of the powder may adversely affect the wetting ability of the melt pool thus hindering densification, and pores may block the irradiation of the raw powder around them which further exacerbates the densification. Therefore, spatter within the process and used powder may result in internal defects like pores and lack of fusions.

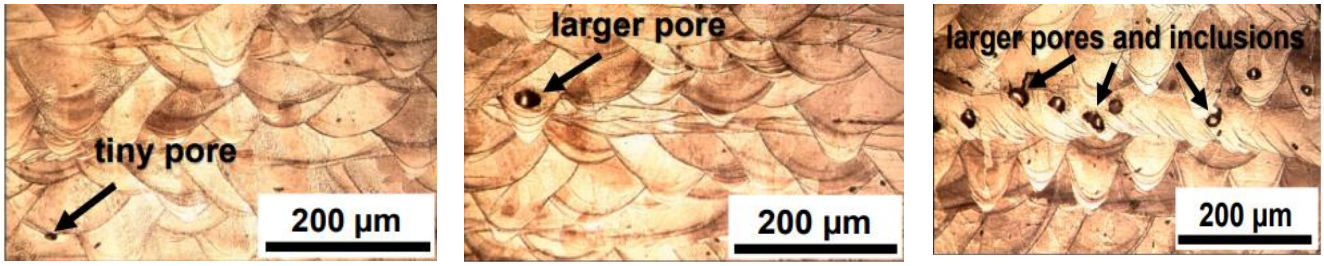

Figure 15 Pores in parts after 1, 3 and 6 times used powder.[21]

Pore formation is demonstrated in the Figure 15, amount of the reuse of the powder directly correlates with frequency and size of the internal defects. Such relation is also significant with the performance of the parts built when tested under tensile stress. Process stability is tested when the inert gas circulating systems power is reduced therefore unable to move away the size of the spatter that are bigger than average. Experiment results show that tensile strength, yield strength and elongation of the parts built with the powder that is being used for 6^{th} time, drop by 30%, 20% and 70% respectively in comparison to the parts built with virgin powder.[21]

Figure 16 gives an example of relatively more extreme occurrence of spatter formation during SLM process. Gas flow direction is indicated and accumulation of spatter are marked. While building a part which has large cross section s has it exposed, amount of spatter formed and transported by the inert gas flow inside building chamber also increases. As it can be seen the zone to which spatter are moved, also overlaps with the cross section of the part that is being exposed. At the overlapping zones the process might have the tendency to form inner defects. This phenomenon shown here points out two aspects of the SLM process regarding its complexity. Firstly, the cross section al area of the parts exposed effects the amount of the spatter formation and also effect the quality of the parts located at the downstream of the inert gas flow in relation with the location of big parts is important. The same applies for when there are a lot of parts located on platform. Secondly, even though, the dimension of the part is within the building platform and the possible Z height that can be built, accumulation of spatter and its effect on the final quality of the part should be considered. In addition, the higher the Z height of the orientation of the parts, the higher the possibility of the defect formation. This is due to possible instabilities that would be introduced to the same zone continuously throughout the entire process.

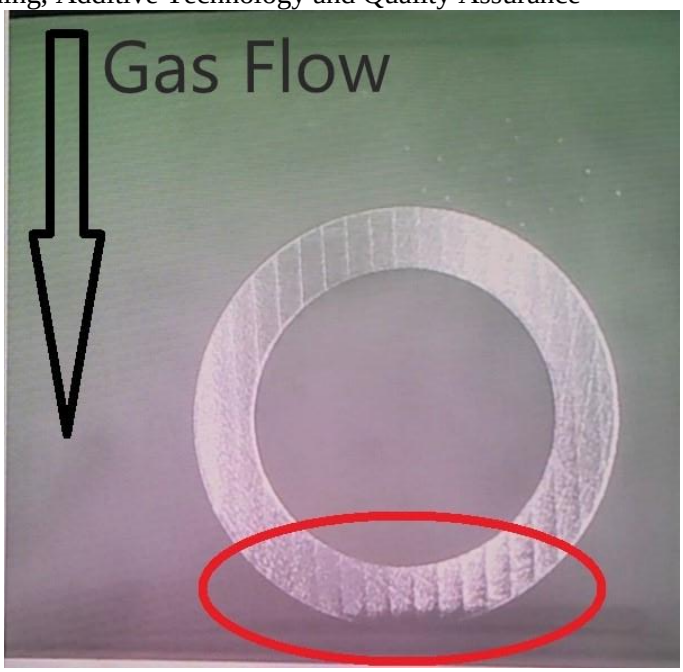

Figure 16 Top view of the building platform and accumulation of spatter particles with respect to the inert gas flow direction.

2.1.4.3 Residual Stresses

SLM process relies on melting of material in high scanning speeds, thus inherently creating the thermal gradients within the parts. Owing to that large thermal gradients, SLM also generates large amount of residual stress. So called, Thermal Gradient Mechanism(TGM) introduces residual stresses to the parts, even though TGM does not require material to be melted.

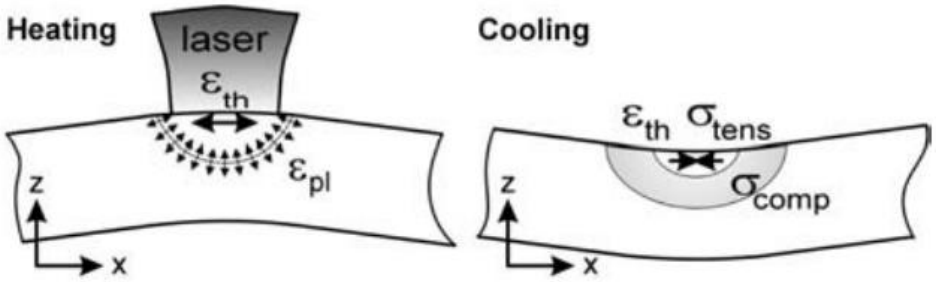

Figure 17 Temperature Gradient Mechanism and compressive and tensile stresses during melting and cooling.[23]

Figure 17 shows the working of TGM. When the top layers of a part are heated and melted by the rapid heating of the laser beam. The top layer expands however compressed by the previously built and consolidated layers which is leading to elastic compressive strains due to expansion being restrained. As the expansion continues these heated layers gets plastically deformed. On the other hand, during cooling plastically deformed layers start shrinking therefore leading to tension within them and deforming upwards. Finally, TGM results in tension forces at the top of the parts and compressive forces within below.[23]

The TGM introduces residual stresses to the parts as explained, however such residual stresses may lead to several outcomes for a part, namely, deformations, crack formation and lowering mechanical strength. And also the residual stresses are released in the form of deformation of the parts while they are being cut off building platform.[24]

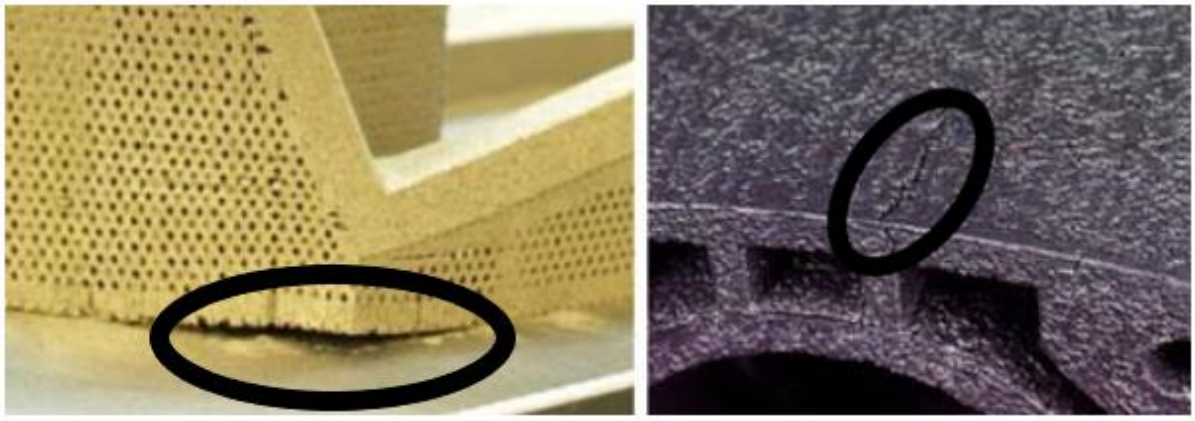

Figure 18 Deformations during and after SLM process and possible crack formation[24]

When different scanning strategies applied to observe the changes in amount of residual stress based on creating various thermal gradients within parts. The material of selection was 316L for their experiment. 4 different scanning strategies were tested. By line Y strategy laser exposure happens along with the with of the parts' width while line X corresponds to scanning by the laser along parts' length. The other two scanning strategies correspond to splitting the surface into sectors, in other words islands or rasters, and scanning those sectors either successively or randomly. The results of this experiment show that the shorter hatching vectors(Line Y) led to highest amount of tension residual stress between 95-145 MPa and long hatching vectors(Line X) induced the least amount of residual stresses with 5-40 MPa. Random and successive island scanning resulted in similar amounts of residual stresses between 50-90 MPa.[23]

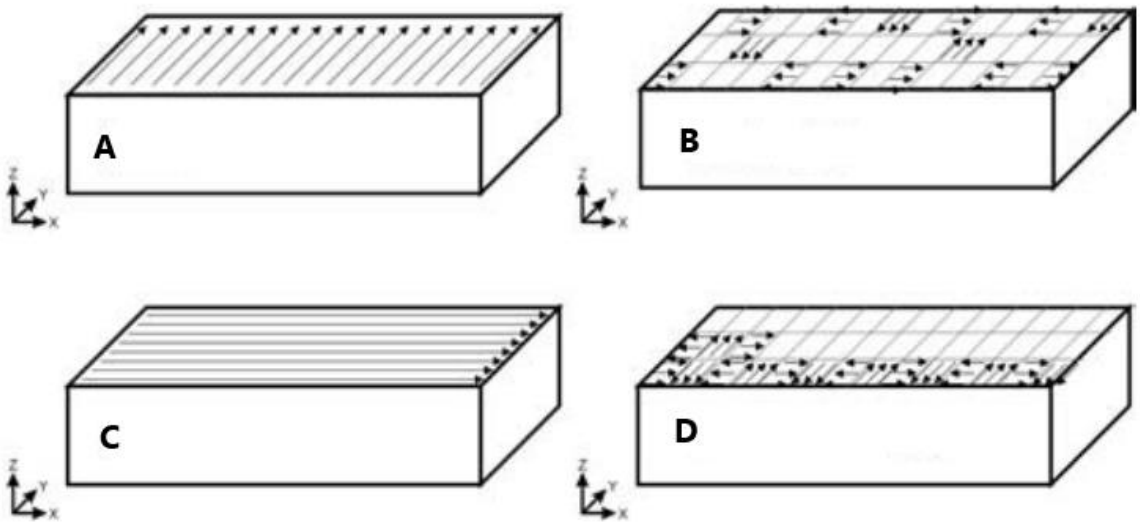

Figure 19 Different scanning strategies tested.[23]

After the melting of separate island on a fresh powder layer, during contraction occurs at the edge of islands. There is no other islands or solidifying material therefore the thermal stress at the border of islands is zero. Later when the successive islands are being exposed the force at the borders increases however it remains lower than that of short hatching.[23]

2.2 In Situ Process Monitoring

In order to meet the demand in the market, SLM technology has shown significant progress in recent years regarding machine construction, production speed, variety of materials used. Despite its evolution one of the main challenges keeping SLM from wider adaptation is quality assurance. Internal defects are formed as explained before and due to layer-by-layer nature of the process, such defects are invisible to naked eye. X-ray computed tomography(CT) can be used for ensuring internal quality of the parts. The disadvantages of CT however are, its high cost, limited accuracy and the limitation of the size of the part that can be evaluated.[25]

Some of the industries where quality and repeatability are very crucial for SLM to be adapted are aerospace and medicine. Based on the fact that each geometry's production is unique with SLM and process cannot be improved to totally eliminate the formation of the internal defects. Furthermore, internal location of the flaws within the parts may also hinder or make it impossible to fix them after production.[26] Evaluation of the process by monitoring systems can be divided into two as online and off-line. Online evaluation refers to real time observation during the process with the aim of interfering with it with corrective measures in the case of flaws forming during production. Off-line evaluation takes place after the print is finished, it requires additional time and it may be used for optimizing next prints.

In this chapter, some of the in-situ monitoring systems developed by both companies and universities will be explained including approaches, components and tested capabilities of such systems. However, data acquired by monitoring system devices should be evaluated with respect to process set up. Due to the fact that changes in the process monitoring data crucially depend on the process settings, in order to evaluate the data process phenomena should always be regarded.

Firstly, to mention the main components for data recording are photodiodes and Charged Coupled Device(CDD) or Complementary Metal Oxide Semiconductor(CMOS) sensor cameras. There are similar layouts tested in industry and research for the purpose of utilizing such components.

Figure 20 demonstrates the In-Line or On-Axis monitoring system setup in addition to laser mechanism for an inhouse built 3D printer.[25] It is important to distinguish the components of the printer. Number 4, referred as laser source output in the scheme is collimator, this component turns the laser light into a parallel beam. Component number 2 is named as scanner with f-theta lens creates the movement of the laser focus on building platform. The laser beam comes through the collimator is reflected by a semipermeable mirror and by scanner directed to the powder bed. The goal of On-Axis systems is the capture the light emitted from the melt pool, because of laser exposure. Reflected light beam goes through scanner and semipermeable mirror and then meets the beam splitter. After splitting the beam, light beam or radiation beam is sent to both photodiode and CMOS-Camera. However, there are also examples of using the CCD cameras in similar setup as shown by.[27] Since the monitoring is done for specific areas that are being irradiated with in-line monitoring it is not necessary to observe the entire building

platform simultaneously. This way, a camera with smaller resolution such as 200 x 200 pixels can be sufficient for detailed observation. And also, focusing to a small area decreases the image size drastically.

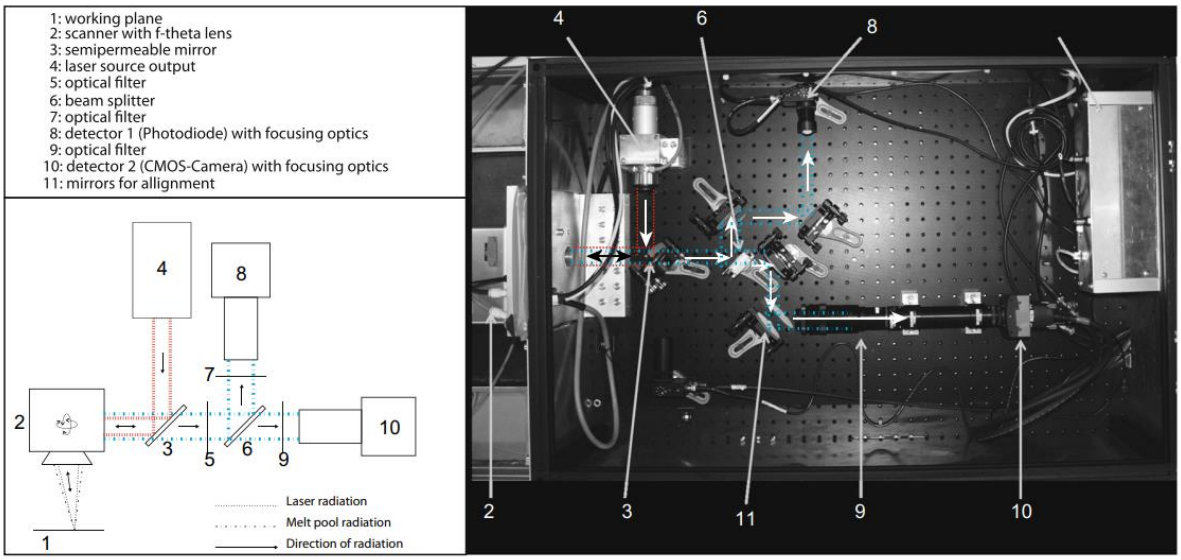

Figure 20 On-axis layout for monitoring with camera and photodiode[25].

There is another approach for using monitoring devices to observe SLM system can be off-axis monitoring. As it can be seen in the Figure 21, this approach installation of monitoring systems may not require direct interfering with the optical components of a SLM machine. Both CCD and CMOS cameras as well as photodiodes can be installed similar to on-axis monitoring. With this approach, compensation for the location of the sensor may be necessary. Such compensation may be in the form of hardware solution such as using tilt and shit lenses and/or in the form of a software where correction algorithms may be used in order to obtain comparable data from every location on a building platform.

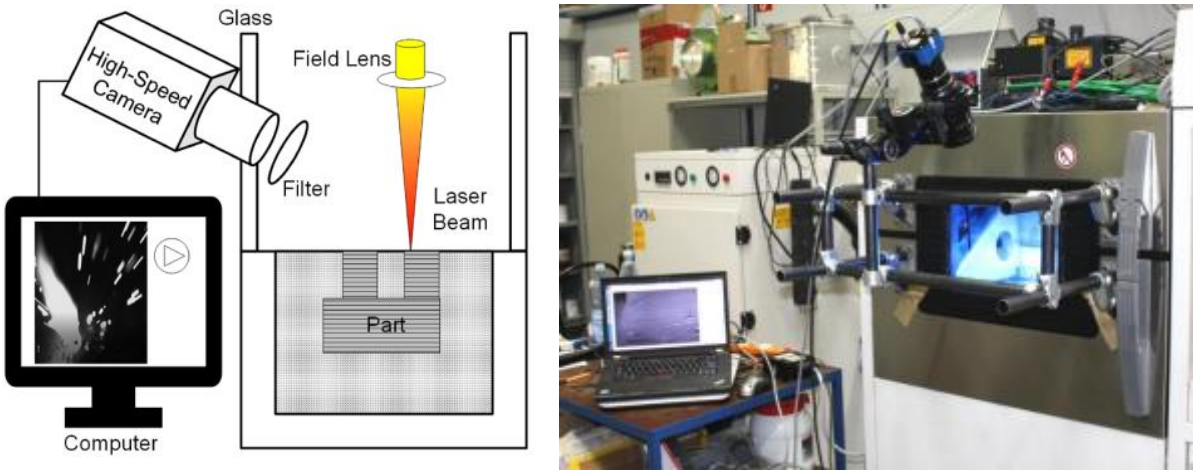

Figure 21 Off-axis observation scheme and application.[21], [28]

2.2.1 Observation by CCD Cameras

CCD cameras are usually used for the purpose of high-speed photography observation. Therefore, for the clarity of the images captured the viewing area should be correctly illuminated. As it shown in the figure 9, additional light sources may be necessary as well as matt reflectors to avoid reflections from surfaces inside the building chamber. In addition, the location and direction of light sources also matter in regards to scanning strategies used as well as highlighting the disturbances on surface of part, e.g dark field light source in this example [28].

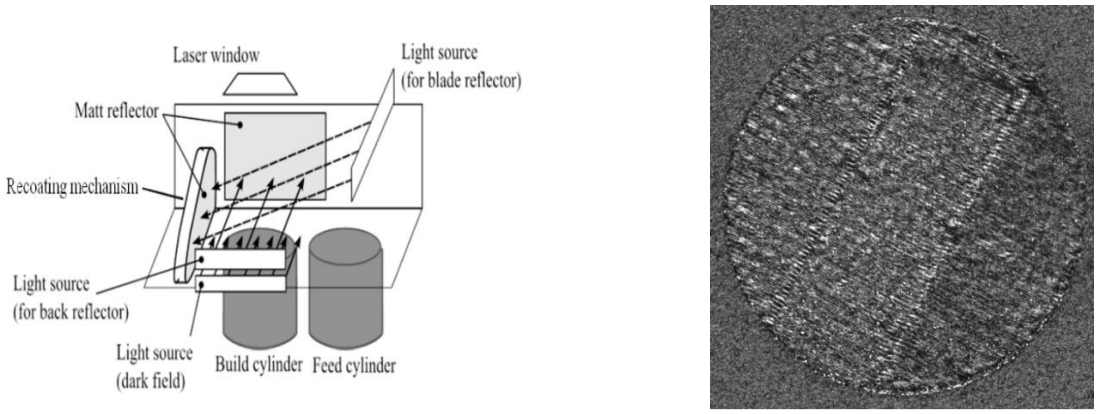

Figure 22 Illumination setup and example image.[28]

Local and temporal resolution are both crucial to ensure observability of all monitoring devices. A CCD camera that observes the whole 250x250mm^2 building platform with 2000x2000 pixels would have the resolution of 125x125 µm per pixel. When the melt pool width is taken into consideration as 150 µm, a melt pool image will be created by using 4 to 9 pixels (Figure 23). Since such resolution is low for recognizing visual characteristics of melt pool such shape, length and width, there can be inaccuracies[26].

$$fps = \frac{v_{scan}}{w_{seam}} \tag{2.2}$$

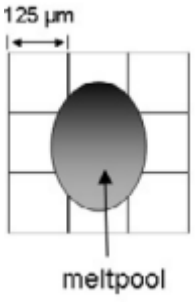

Figure 23 Melt pool size comparison with pixels‘ size[26].

Temporal resolution or Frame Per Second(fps) rate necessary is calculated. W_{seam} refers to melt pool width to be observed. As an example, melt pool width of 150 µm to be observed for the printing with the exposure speed(v_{scan}) 900 mm/s then fps necessary becomes 6000. Therefore, it can be said the for different exposure speeds that are necessary for different materials optimal fps might differ as well.

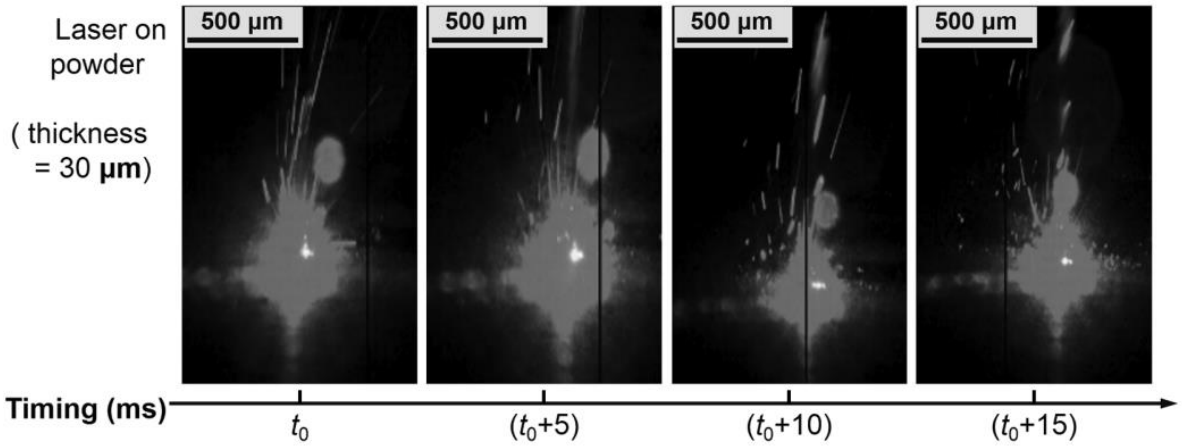

Figure 24 Process monitoring with scanning speed 200 mm/s, 1000x500 resolution and 4183 fps.[21]

Figure 24 gives an example of usage of CCD cameras for process monitoring with off-axis approach. According to temporal resolution formula explained before, for the 4183 fps and 200 mm/s of scanning speed, the melt pool width that can be observed becomes approximately 47 µm. Therefore, it can be said that 4183 fps is more than enough to observe the melt pool since melt pool's size will be bigger than observable melt pool width.

In addition, images in the Figure 24, were observed during printing with a DiMetal-100 SLM machine. This machine has the building capacity of 100x100x100 mm. Therefore, local resolution of this setup can be calculated as 100x200 µm per pixel if we assume camera's view only covers the building platform. However, since in reality camera does not focus only on the building platform, actual resolution is lower and such resolution may not be sufficient to provide information on the details of the melt pool.

In another case study, visual inspection is utilized for the purpose of inspecting recoating of powder bed with fresh powder. Due to thermal stresses, parts can deform upwards or "curl-up" according to TGM which may cause contact with the recoating blade. Such contacts may cause disruption of the recoating and may also result in damaging the recoater blade. In[29], an off-axis setup was used to observe recoating. For this case study since the frequency of recoating is once in every layer, very high frequency of the camera is not necessary.

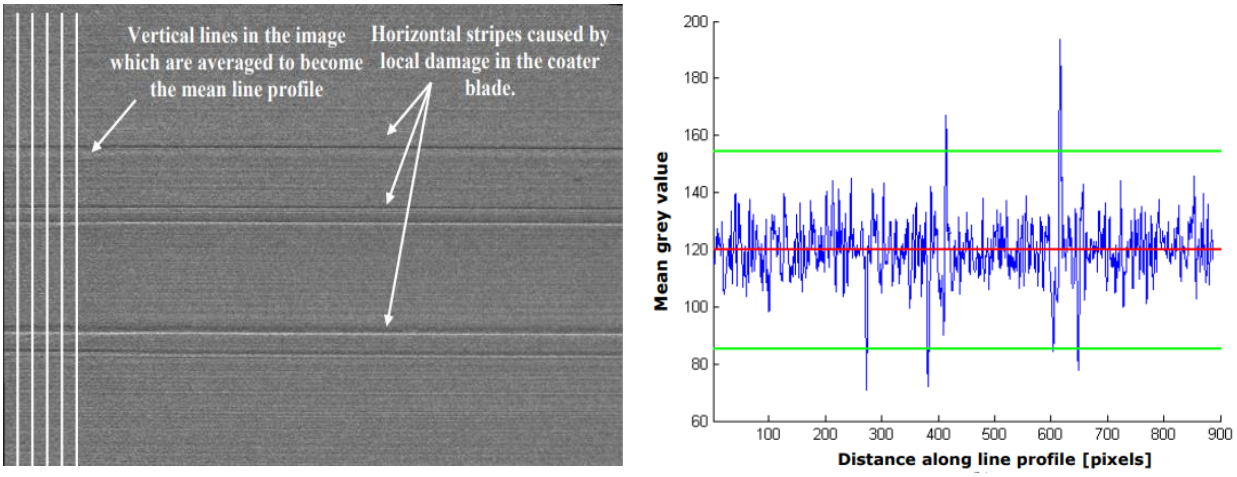

Figure 25 Irregularities in distributed powder layer and grey value signal fluctuations.[29]

Image given in the Figure 25, discontinuities in powder distribution are manifested as horizontal dark lines. Such lines are formed due to local wear on recoater blade. It is suggested evaluation of such imagines in the form of grey values. Vertical lines in the image indicate the data points by which an average grey value calculated and standard deviation is selected based on the actual view of the laid powder. On grey value scale, lower values correspond to darker sports on the layer. With this method disruption of recoating process can be kept under control for every layer.[29]

In conclusion, CCD cameras are capable of providing information about the size of the melt pool and spatter ejections from the melt pool, as well as about powder distribution constancy. However, temporal and local resolution of cameras and hardware setup including illumination should be adequate to the process parameters and conditions.

2.2.2 Observation by CMOS Cameras

Difference between the use of CMOS cameras for process observation with CCD cameras is in terms of data collection and final outcome of the process. CCD cameras are used for creating real life photography of the process where the actual image of the layer or formation of spatters formed observed. According to Planck's law metals emit their peak radiation at melting roughly around 1500 K by near infrared light spectrum. In the case of CMOS cameras, the approach is to collect data regarding the radiation emitted in certain wavelength spectrum from the melt pool in order to evaluate the process stability.[25]

CCD sensors contain array of photosensitive sites that collect data unlike CMOS sensors that use photosensitive pixels. While these both technologies convert light into electrical charge CMOS sensor collect the data digitally in comparison to analog process of CCD, therefore CMOS sensors have higher frequency (10 kHz) with lower sensitivity which results in noisier images. In contrast, CMOS cameras are more sensitive to infrared radiation wavelengths (0.780-1 µm) that CCD sensors. [7]

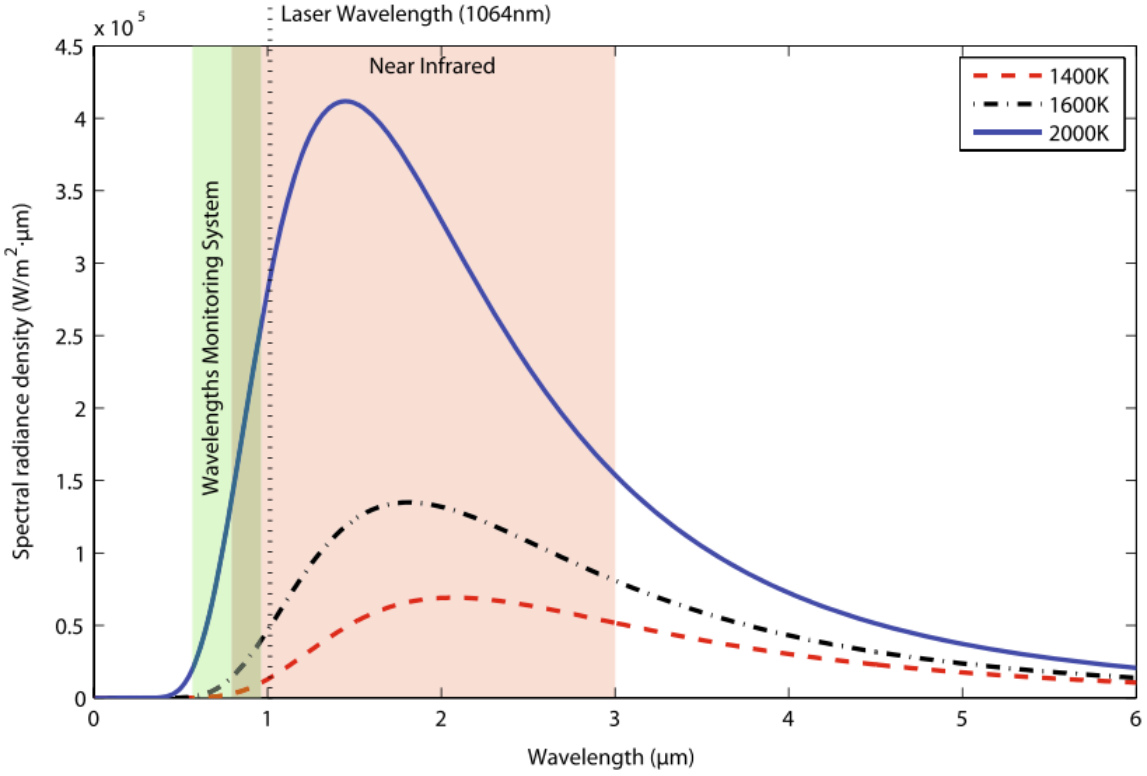

Figure 26 Wavelength ranges involving laser, monitoring systém and near-ifrared spectrum. [25]

In Figure 26, the wavelength spectrum at which CMOS camera aimed to collect the data based on the reflected radiation from the melt pool. This spectrum is selected based on multiple factors. In the setup of [25], ytterbium laser with the wavelength of 1064 nm is used. The laser is reflected with semipermeable mirror(figure 7, component 3) which is coated for 100% reflectivity for the wavelength of 1000 nm. Therefore, the wavelength of the light that can go through the semipermeable mirror and get collected by the sensor is in a spectral distance from the full reflectivity of the mirror. Thus, upper limit is selected as 950 nm. In order to avoid the affects of the process chamber illumination and reflections which have the highest wavelength of 700 nm, the lower limit is selected at 780 nm.[25], [30]

Figure 27 demonstrates a relatively new approach to process monitoring. Monitoring systems focus on behavior of the melting pool and data recorded can be plotted as a function of time and as well as function of space. In an example, mapping of the melt pool data in X-Y plane by a function of space is given. As explained before, according to the frequency of the monitoring sensor and the approach of the setup(in-line/off-line), data gathering frequency as well as the amount of data points are changing. With this mapping approach, data points recorded are assigned to nearest pixel. And since the color of pixels correspond to the magnitude of the data assigned to that pixel, an image is created for each layer of the process[27].

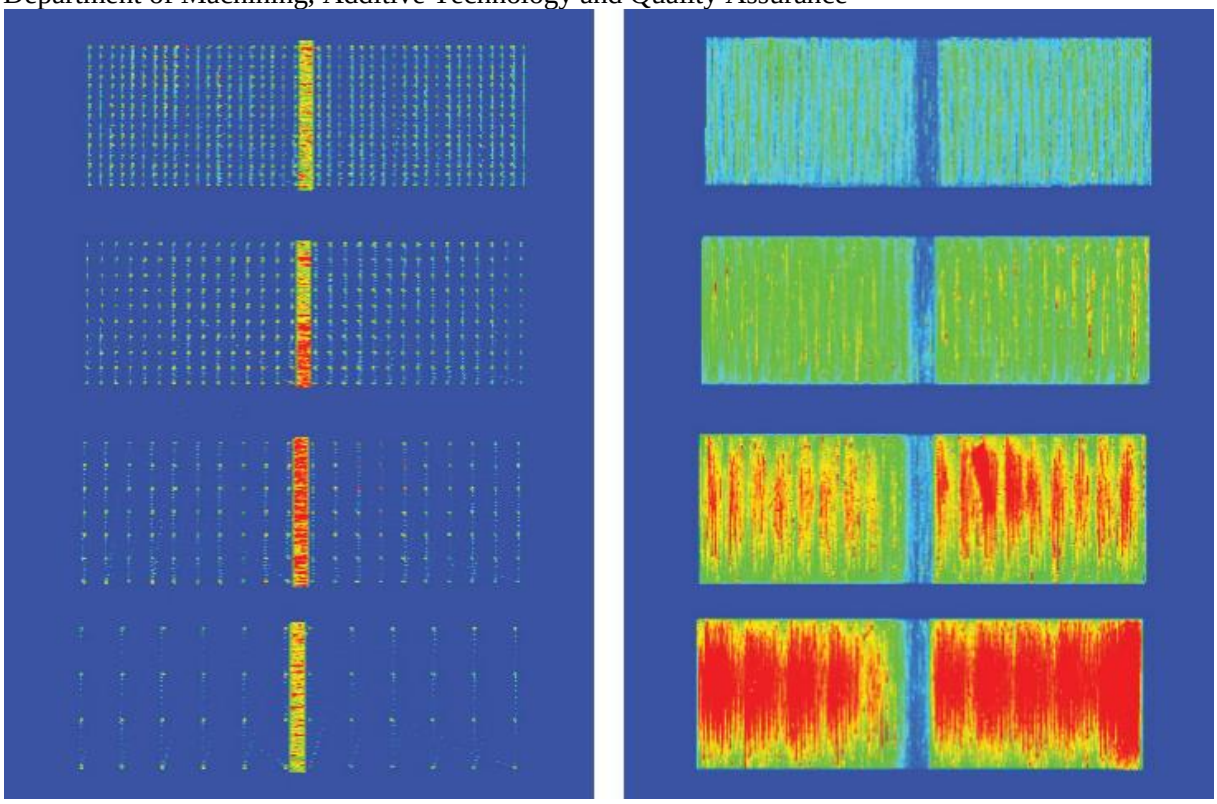

Figure 27 CMOS camera signal map for a T-shaped part for different amounts of supports used.[27]

In the Figure 27, example of the data collected and mapped. This map was generated by taking the average of the data that is assigned to each pixel. T-shaped parts were built with different amount of supports beneath overhang surfaces. The density of the support structures is visible in the first pictures. The difference between signal intensities in the images while overhang structures are being built points out differences in the conduction rates. Conduction to the building platform through supports directly affects the melt pool behavior. And due to the differences in the intensity changes, it can be said that lower amount of supports led to lower rate of conduction thus resulting in higher temperatures reached during melting of the material.[27]

2.2.3 Observation by Photodiodes

In this subchapter optical observation by the utilization of photodiodes will be discussed. Similar to other devices explained before photodiodes can be used coaxially or in-axis with laser or off-axis. Photodiodes can reach the sampling rates of 10 kHz, similar to the cameras or higher. While photodiodes are susceptible to variations within SLM process and can provide significant data, these devices are also utilized as complementary tools to cameras in many different experiment designs.

Usually, the data gathered by photodiodes are plotted with time domain. In this example, two photodiodes are used in the form of a pyrometer. While aiming to observe melt pool behavior and explains the trends within the curves with regards to melt pool mechanics, process setting and optical superposition. SLM machines calibrated for deposition of heat into a fine spot, however both heat-affected zone and actual melting radius are larger than that of laser spot. By selecting the hatching spacing carefully, continuous melting between the melting tracks are

aimed. Photodiodes with this set up, gathering data with the principle of optical superposition which means the overlaps between the heat-affected zones of multiple melting tracks lead to algebraic sum of the data recorded.[31]

Pyrometer signal is shown the Figure 28 , demonstrates the effect of optical superposition. Data in this figure is recorded during exposure of subsequent melting tracks. Due to sum of the data, the mean of the curve increasing with the increasing number of tracks exposed. On the other hand, Figure 28 also demonstrates the effect of various hatch spacing parameters selected on the data. It can be seen the wider hatch spacing leads to lower signal and shorter time for exposing the same amount of surface while it is the other way around for smaller hatch spacing.

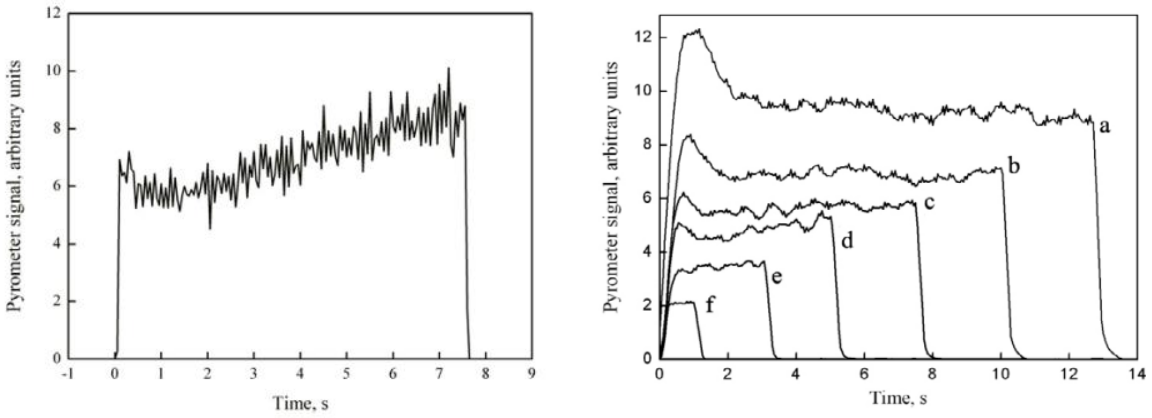

Figure 28 Pyrometer signal for hatch spacing of 120µm, and pyrometer signal comparison for hatch spacings of 70(f),90(e),120(d),180(c),300(b),1000(a) µm. [31]

Another example of using photodiodes for ensuring process reliability is shown in Figure 29.[26] In this example the mean of photodiode signal amplitude and standard deviation is calculated for each layer. Due to problematics in the movement of the building platform powder supply was also hindered. At this example, at the layer 1600 building platform gets stuck therefore a new layer of powder cannot be laid over the platform for 400 layers, and later platform moves down for 400 layers at once. Loose powder's heat conduction rate is very small in comparison to solid material. This leads to heat being trapped at the top of a very thick powder layer, thus melt pool emits more amount of light which is captured by photodiode.

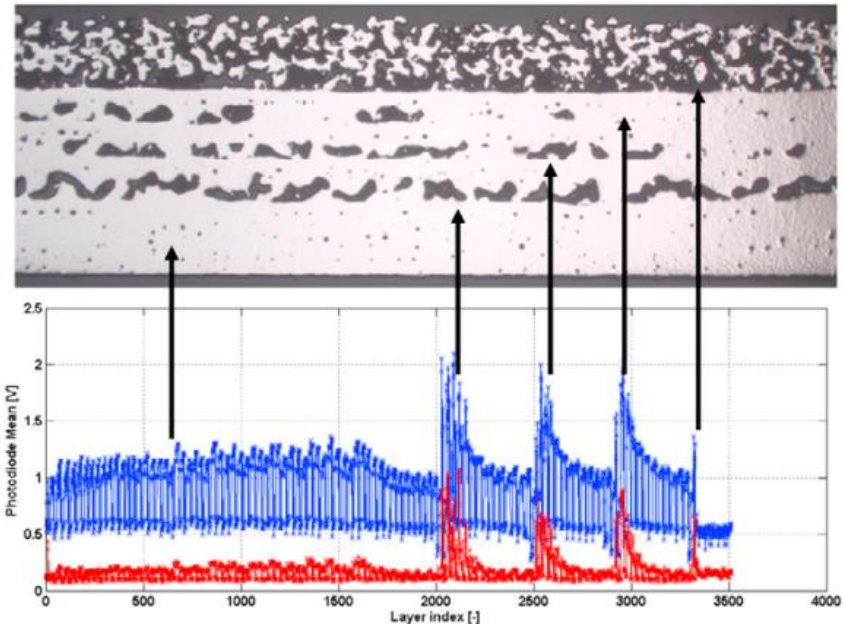

Figure 29 Building platform's error and it manifestation on building layers and monitoring signal.[26]

3 Proposal for Design and Realization of My Experiments

Main mechanisms of SLM and some of the factors which has significant effect on the final properties of parts produced has been discussed so far. In addition, in situ process monitoring devices and data evaluation methods has been explained. With the goal of regulating some of the process phenomena, observation by monitoring systems and evaluation of mechanical properties of the parts corresponding with the monitoring data, series of experiments has been designed. For this work state of the art EOS M290 machines, EOSTATE Monitoring Suite and exposure strategies patented by EOS GmbH were used. In addition

3.1 Experiment Equipment

3.1.1 Machine

For production of the parts, state of the art M290 Metal printing machine was used. This machine is one of the most commonly used systems in the world. One of the most important aspects of this machine regarding the aim of this work is the possibility of installing monitoring systems.

Figure 30 EOS M290

A M290 can be used for printing 24 different materials ranging from stainless steels, Nickel alloys, Titanium based alloys to tool steels. SLM processes are defined by EOS for each material based the layer thickness therefore productivity, while aiming for production of dense parts. In addition to the process settings developed by the manufacturer, different recoating options are also provided. Recoater blades can be made of High Speed Steel(HSS), ceramic, silicone or in the form of carbon fiber brush. The type of recoater blade to be used is selected based on the desired repeatable quality or the flexibility of the process. And also, machine is capable of creating inert gas atmosphere using Argon gas supply or filtering out the Nitrogen in the air. The type of inert gas atmosphere is selected based on the material. Technical information of this machine is given on Table 1.

Table 1 Technical data of EOS M290.

Building Volume	250x250x325 mm
Laser Type	Yb fiber laser; 400 W
Precision Optics	F-theta lens; high-speed scanner
Scanning Speed	Up to 7.0 m/s
Focus Diameter	100 µm
Power Supply	32 A / 400 V
Power Consumption	Max 8,5 kW
Compressed air supply	7000 hPa ; 20 m^3/h

3.1.2 Material

Material choice of use for this work is EOS Maraging Steel MS1. This material has the chemical composition of %18Ni Maraging 300 according to US classification and 1.2709 according to European system.

Table 2 Chemical Composition of EOS Maraging Steel MS1 .

Element	Ni	Co	Mo	Ti	Al	Cr	Cu	C	Mn	Si	Fe
Content (wt-%)	17-19	8.5-9.5	4.5-5.2	0.6-0.8	0.05-0.15	≤0.5	≤0.5	0.03	≤0.1	≤0.1	Balance

MS1 is a tool steel with good mechanical properties, easily machinable and heat treatable. According to the machine manufacturer, it can be treatable by age-hardening to obtain hardness more than 50 HRC. And both as-built and age-hardened, parts built with this material can be spark-eroded, welded, micro shot-peened, polished and coated if desired. Ceramic recoating blade and nitrogen atmosphere is selected for this material.

As mentioned before layer wise building method of SLM results in certain amount of anisotropy. According to the EOS GmbH, solution treatment of this material at 940 °C for two hours can reduce or remove the anisotropy developed during process. 40 µm layer thickness process defined by EOS is used for this work. And, with the aim of observing the results of utilizing different scanning strategies, solution treatment of the parts built was avoided.

One of the purposes of the experiments designed is to evaluate the behavior of this material with respect to its tendency to deformation, heat conduction, cooling rates and susceptibility of the changes in the exposure strategy.

3.1.3 Monitoring Systems

As mentioned before EOS M290 machine can be equipped with monitoring systems and EOS provides multiple monitoring systems under the name of EOSTATE Monitoring Suite. This monitoring packaged contains three different in-stu monitoring systems namely, PowderBed, Optical Tomography, Melt pool Monitoring. In this subchapter the approach and working principles of these monitoring systems will be explained in relation with the chapter 2.2 In Situ Process monitoring.

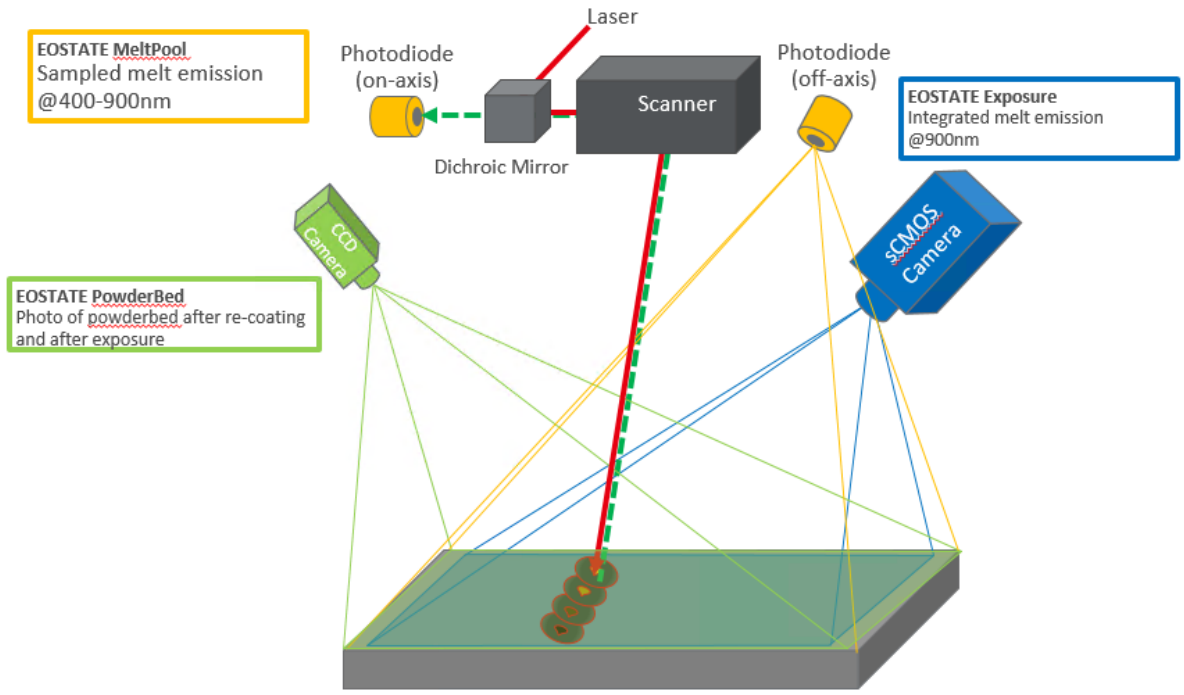

Figure 31 EOSTATE Monitoring Suite setup. The graphics in this figure was provided by EOS GmbH during monitoring systems training.

EOSTATE Monitoring systems utilize the device or sensors such as photodiodes, CCD and CMOS censored cameras. To lay the groundwork about these devices, different approaches regarding the use of them were explained before. EOSTATE systems use such methods in such a way that combines the use of multiple sensors in order the carry out quality assurance during and after the process.

To begin with the PowderBed, this system utilizes a CCD camera in an off-axis setup as it can be seen in the Figure 31. The use of this camera with this setup however is different than examples from the literature that were shown previously on this work. Instead of following the melt pool behavior, in this case CCD camera is used to ensure that they are no discontinuities with the recoating and powder is distributed evenly throughout the building platform. It captures only a few pictures of the platform during print of a layer therefore high frequency is not necessary.

Secondly, Melt pool Monitoring(MPM) system employs two photodiodes while one being on-axis with the laser the other one is positioned off-axis. This way, both co-axial and lateral light emitted from melt pool is captured. The MPM, sampling frequency can be up to 60 kHz. Unlike the examples of utilization of photodiodes in the literature that were shown before, MPM generates both time domain plot for each data point from a layer as well as space domain view on building plane as it can be seen in the Figure 32.

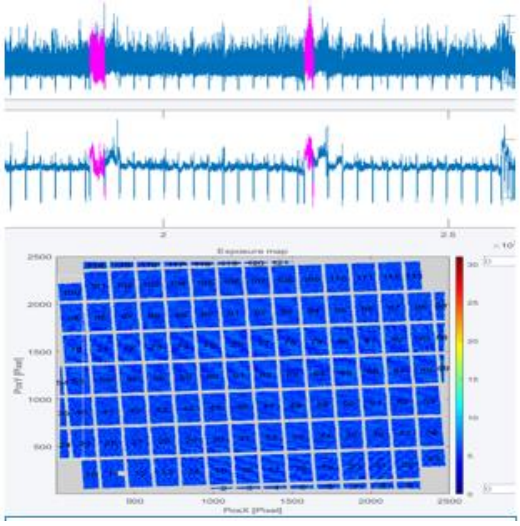

Figure 32 Example of data visualization by EOSTATE MPM.

Powderbed and MPM systems were explained briefly. The focus of this work regarding monitoring systems will be on Optical Tomography(OT). OT exploits a CMOS censored camera that is placed off-axis. This camera has 145 µm of resolution per pixel and it captures the light in wavelengths around 900 nm. Due to camera's placement, unlike an on-axis setup, based on location of a data point on building platform data recorded differs. This is solved by software correction.

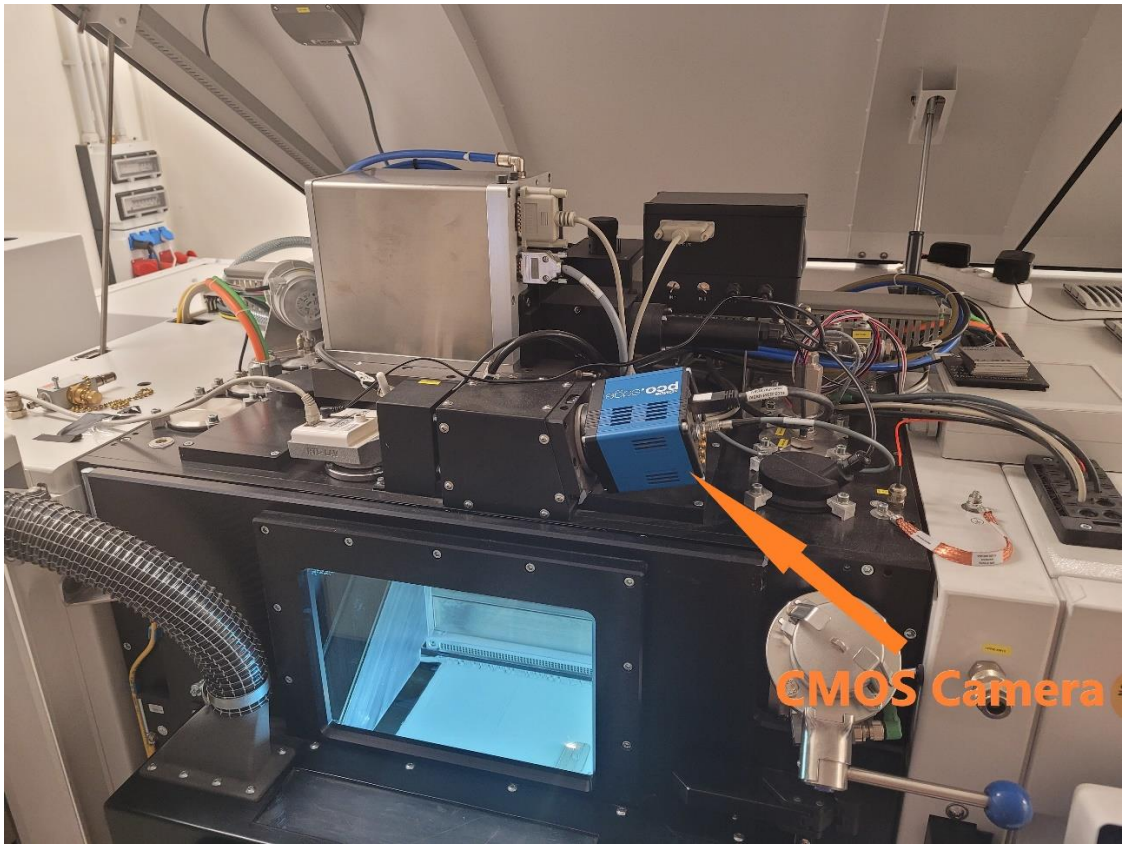

Figure 33 Mounting of CMOS Camera on EOS M290 machine that is utilized for this work.

There are multiple outputs of the data recorded by OT. Firstly, in the form of a curve that visualizes the data recorded for each layer during production. The unit for the data recorded due to radiation emitted from melt pool is called Grey Value(GV). The curve created based on mean GV throughout building height of parts(Figure 34). This output from OT might gives significant amount of information based on process dynamics. Similar to, the previous examples of monitoring system outputs, trends in the curve may correspond to the heat input on a layer and conduction rate on the particular point during building a part.

In addition, the standard deviation of the curve refers to changes in every layer specifically. On the chapter 2.1.3, the shift and turning of the scanning strategy in between each layer was mentioned. Due to such differences in the way of heat input on each layer, GV recorded may also change. Especially, in the case of thin-walled parts such changes become visible in the GV curve therefore resulting in bigger standard deviations.

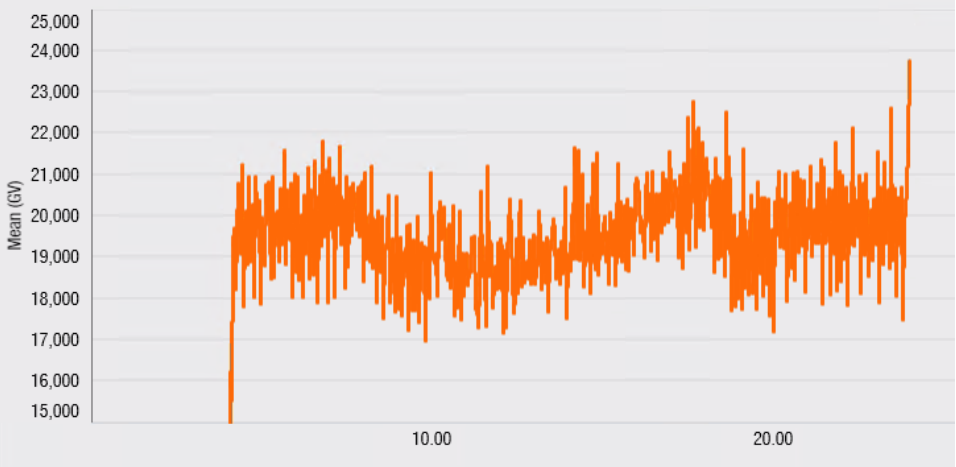

Figure 34 Mean GV curve example according to the building height.

OT also provides GV value map of each layer where the data is presented on a plane as well. However, OT uses two different approaches for the data output.

Figure 35 OT maximum value image imagine example.

Firstly, maximum value image demonstrates the momentary changes during exposure of a layer. Which means a data point on a layer assigned by only one amplitude of GV and it presents only this value as well. Therefore, any momentary change, whether a peak point in the data or lower data is captured and presented as it is. In addition, maximum image also results in the optical phenomenon called “ladder effect”, according to the sampling frequency of the CMOS camera and scanning speed of laser, the exposure map is divided into islands or steps of data recorded.

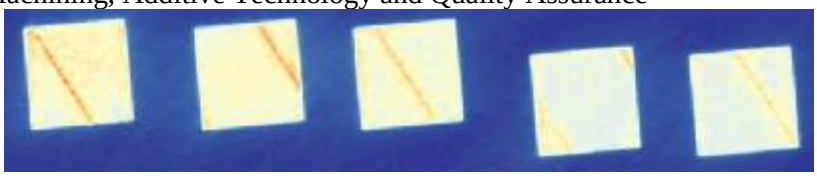

Figure 36 OT integrated value image example.

OT integrated image is created in a different way. Like optical superposition that is mentioned before, integrated image consists of multiple pixels that contain algebraic sum of multiple data points in time domain. In general sense, a pixel can provide data of multiple data points within itself. In the case of maximum value image, the highest data recorded by any of those data points is demonstrated. On the other hand, integrated value image, demonstrates the sum of multiple data points and every single data recorded by these data points throughout the exposure of an entire layer. Therefore, it can be said that integrated image shows the heat input map according to a time frame in which the radiation from melt pool reaches the near infrared wavelengths that can be captured by CMOS sensor.

Since the differences in working principles of images generated by OT explained, evaluation of these images can be discussed too. The parts shown in Figure 35 and Figure 36 were both built with the scanning strategy provided by EOS which his called stripes. The basics of this strategy was explained in 2.1.3 Process parameters. In maximum image islands of data combine invoking the shape of stripes, these islands can be said to be created in the same length of a time window. In the integrated image the shape of stripes is emphasized by the overlapping zones of stripes. Since overlapping zones exposed twice during the scanning of a layer, sum of the data gathered results in red lines pointing out these zones. Nevertheless, such red lines may not necessarily indicate higher temperatures reached.

In conclusion, integrated image may provide information about process phenomena that takes place in a time frame while maximum image marks the momentary fluctuations within the process.

3.2 Design of Experiment

Process understanding of SLM has been significantly increasing as well as adaptation of this process as a mean of manufacturing, such developments lead to and driven by better tools for manipulation of the process. This work was inspired by observation of the process phenomena by OT monitoring system and aspires to investigate the results of relatively new process manipulation tools.

Firstly, one of the things were observed by OT was the susceptibility of thin-walled parts to changing heat input throughout the building height. Figure 37 demonstrates the map of radiation from multiple subsequent layers of the same parts. As it can be seen here, every layer seems to have variations of the signal. This can be contributed to the turning and shifting of scanning strategy in between layers. Especially, while exposing a layer with relatively small surface area, the variations in the length of the hatching vectors may be the cause of changes in the radiation emitted. If there are not any major changes in the part geometry the conduction rate between subsequent layers may be considered the same. Since conduction rate does not change significantly, the variations in the radiation map can be contributed to the variations in heat input.

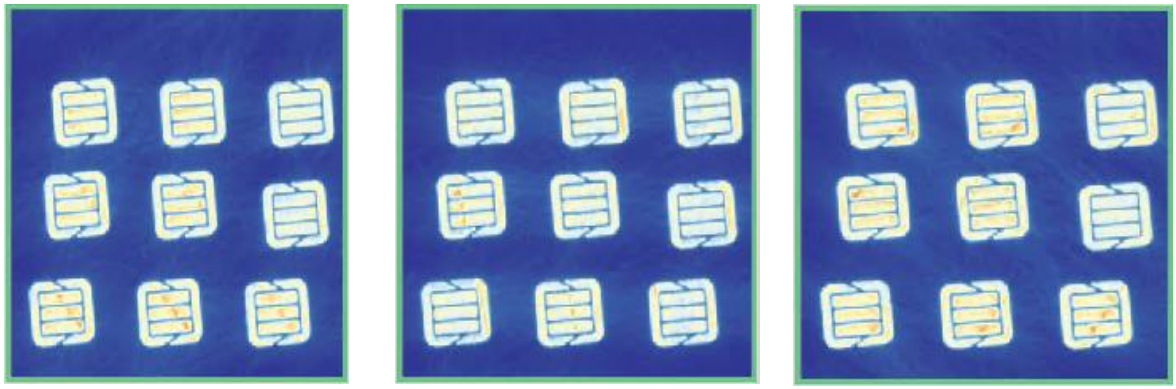

Figure 37 Integrated images of thin walled parts built and observed in University of West Bohemia.

Affect of the both surface area and the changes in the geometry of the parts reflect on the grey value curve of OT. Green curve on the Figure 38 represents a part which is has the same cross section of 10x10mm, all along the building height. While yellow curve corresponds to a part which has smaller cross sections and geometry is changing along building height. First of all the amount of standard deviation on yellow curve is visibly higher, this happens, since the most of the hatching vectors‘ length is changing depending on the exposure angle. Part thickness is 1.3 mm while narrow width of gauge length is 2 mm. Between subsequent layers exposure strategy is shifting by the half of stripe width while turning for 67.7 degrees. In addition, as the cross section of the part becomes smaller, shorter hatching vectors lead to higher standard deviation on second zone of the curve. On the other hand, while building a part with 10x10 mm, the ratio of the short vectors to overall amount of hatching vectors is lower. Therefore, it can be said only thin walled parts might be susceptible to such process variation.

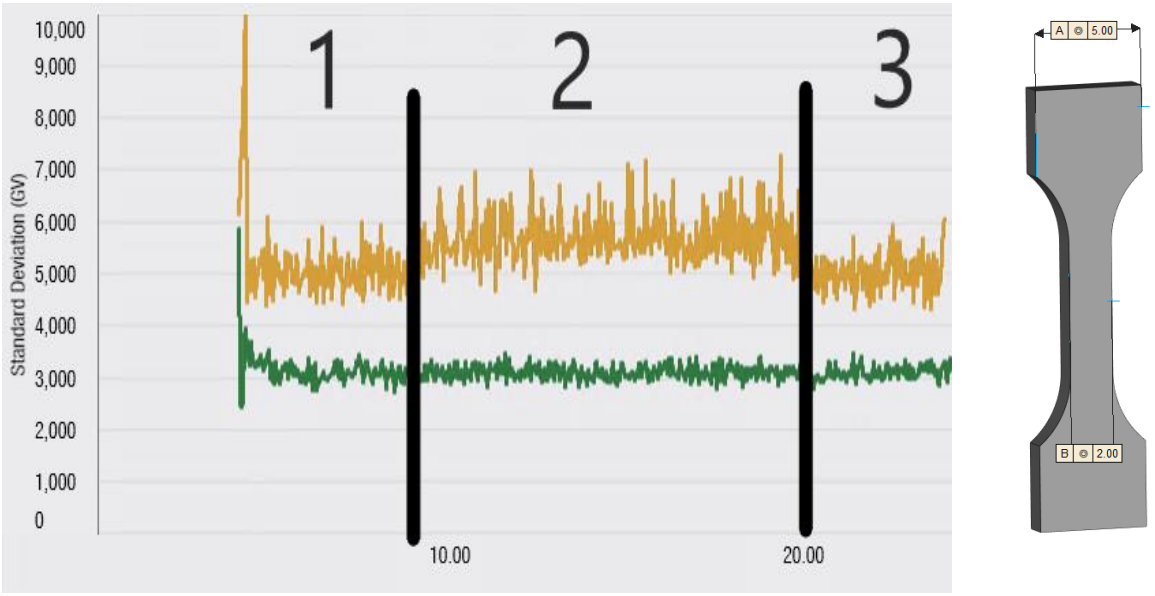

Figure 38 a) Standard Deviation curve of GV plot for parts with two different geometries. b) Geometry of the part with yellow curve.

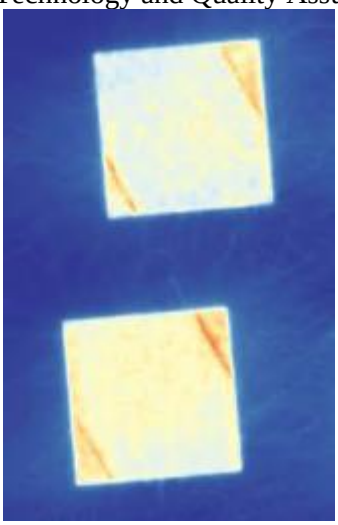

Figure 39 Inhomogeneous heat input due to laser interaction with smoke and plasma above melting pool.

Another phenomenon that was visible to OT, is the interaction of the laser beam with side products of melt pool, such as plasma and smoke that are formed above melt pool. This leads to laser beam defocusing or scattering therefore non-uniform heat input to surface of the part. Such mechanism leads to shallower melt pool thus potentially internal defects such as lack of fusion and balling.

Such observations and phenomena that are visible to monitoring systems are the base for the tools and strategies that are used in this work. Exposure strategy tools to be used in order to avoid failures during prints and optimize mechanical properties of parts built. Effects of manipulating the SLM process will be investigated with the monitoring systems and testing.

3.2.1 Exposure Strategies

In this subchapter, exposure tools that are used in this work will be explained. First aim of the tools will be providing continuously consistent heat input to the parts regardless of geometry of each layer. Secondly, the aim will be to investigate the phenomenon of defocused laser. Therefore, manipulation of the interaction of melt pool with the inert gas flow will be tested.

Scanning strategy is the main mechanism that is dictating the heat input on a layer. Figure 40 demonstrates the tools for energy input homogenization. These tools are defined by EOS and are activated on EOSPRINT software which is used for data preparation of SLM applications.

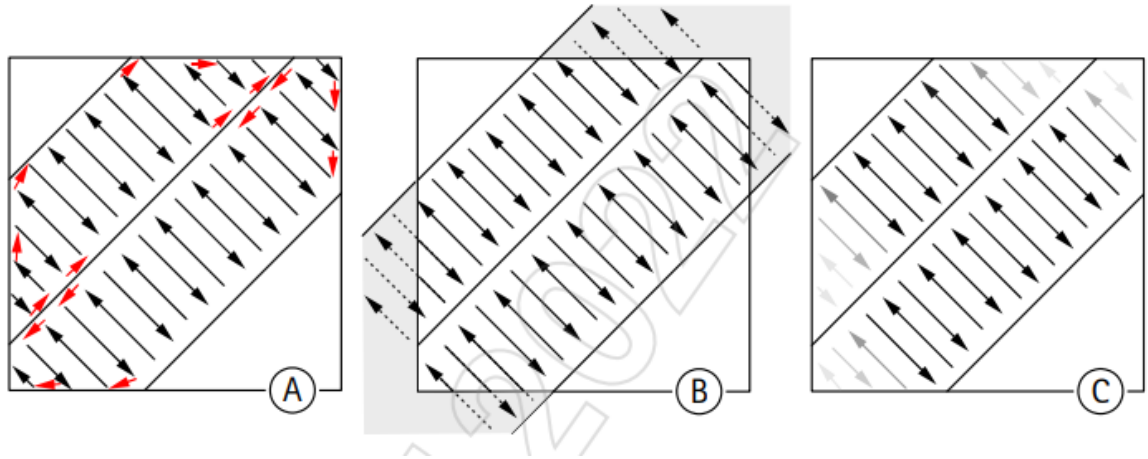

Figure 40 Default scanning strategy and energy input homogenization tools based on EOSPRINT manuals.[32]

The stripes scanning strategy is mentioned before, Figure 40-a represents the default stripe strategy. Initially, it should be made clear the term "short hatching vectors'' refers to any hatching line in the strategy that is shorter in length than that of stripe width. For 40 µm layer thickness MS1 process defined by EOS, the stripe width is equal to 10 mm, scanning speed is 960 mm/s, while the laser power is 285 W and the hatch spacing is 0.11 mm.

The crucial aspect of default strategy is the time frame in which the hatch vectors are applied. Since the scanning speed is the same regardless of the hatch vector length, larger amount of heat is applied with the subsequently exposed short hatching vectors. If a hatching vector's length is equal to stripe width, neglecting stripe overlapping rate, the time necessary for the exposure of the vector can be found by dividing the stripe width by the scanning speed. For this work it can be calculated as 10.41 microseconds based on MS1 process.

Figure 40-b represents the tool which is called "Time homogenization". The aim with this tool is extend the time frame at which short hatching vectors are exposed. Time homogenization introduces waiting times between vectors. Although it does not change the scanning speed, by introducing the minimum time for each vector, time frame on which each vector is applied remains the same. In other words, instead of continuous melting of subsequent short hatching vectors, melting is interrupted between vectors.

Figure 40-c shows the "Power Reduction Factor", with this function short hatch vectors are exposed by using smaller laser power setting. Therefore, it has a different approach for avoiding heat accumulation. In this work, 20% power reduction is selected and the reduction in laser power is done linearly in relation with the length of hatching vectors. Thus, laser power is 285 W for longest hatching vectors while it will be 228 W for the shortest vectors.

Another strategy that is tested in this work is not directly related to heat input homogenization. This function is called "Flow optimization" and utility of this tool is to minimize laser defocusing. As a result, however it provides more uniform heat input that is also observable by monitoring system OT.

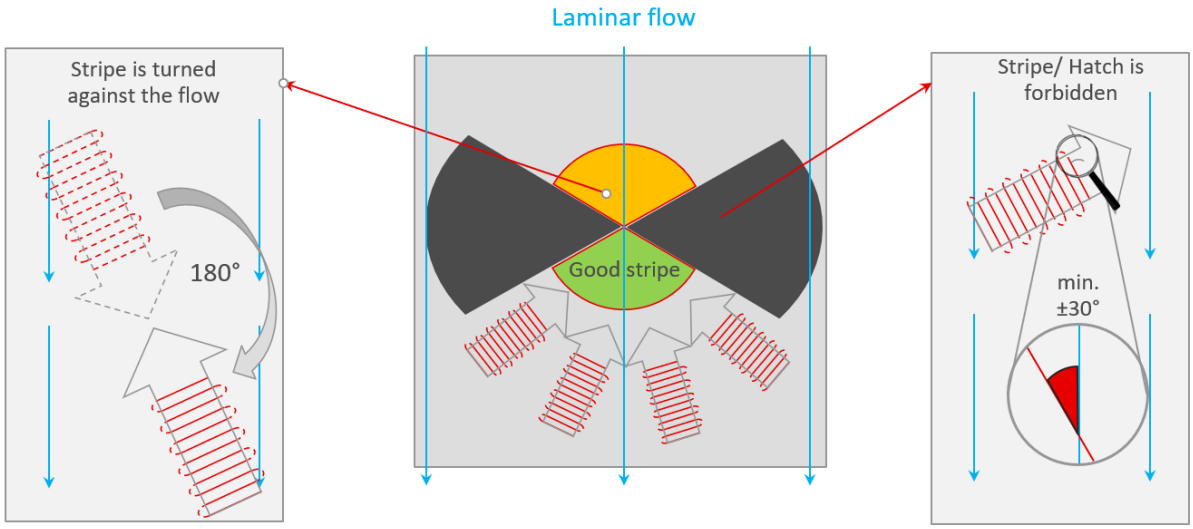

Figure 41 Flow optimization function and directions of stripes and hatches relative to the direction of laminar inert gas flow inside building chamber. The graphics in this figure was provided by EOS GmbH during monitoring systems training. [33]

Hatches are exposed perpendicular to the stripe direction as explained before. Smoke and plasma created by melt pool can affect the hatch vector that is being expose, because of this reason hatch vectors' direction should not be aligned with the inert gas flow. Such hatches are avoided by restriction angle setting that "forbid" exposing them. In addition, those side products of melt pool can also influence the hatch vectors that will be exposed next. Therefore, also the stripe direction should not be aligned with the gas flow. Flow optimization avoids the alignment of stripe by only printing them against inert gas flow.

3.2.2 Part Designs

Parts with various geometries has been printed. One of the main goals was to induce short hatching as much as possible while parts' dimensions are suitable for testing. This was done while also regarding buildability of the parts. Which means while a potentially instable experiments designed for the purpose of observing SLM process phenomena, possible deformations of parts, recoating forces and heat conduction were taken into consideration.

Part in the Figure 42, is the part designed for different measurements. Its thickness is selected as the smallest thickness that can be reliably drilled for deformation and residual stress measurements. Such small thickness results in short hatching vectors in every layer. Direction of measurement is selected, due to the fact that shorter hatches are usually formed near edges of parts. 20 of these parts are built for residual stress measurement. In addition, 4 were built for inspection by light microscope, micro-hardness and SEM images.

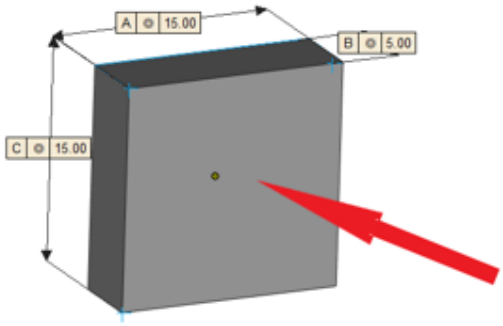

Figure 42 Part designed and tested for micro-hardness, residual stress and metallographic evaluations. Red arrow refers to testing direction for all these tests.

Another part that was built for this work was mini-tensile bars. A part with small cross sections would induce more short hatchings, therefore the affect of tools used could become more significant. Thickness of the parts are 1.3 mm thus smallest cross section, during gauge length is 1.3 x 2 mm. However, in order to build such parts, prop supports were required. With the goal of increasing conduction rate as well as introducing additional stiffness, prop shells were designed. These were removed after the print.

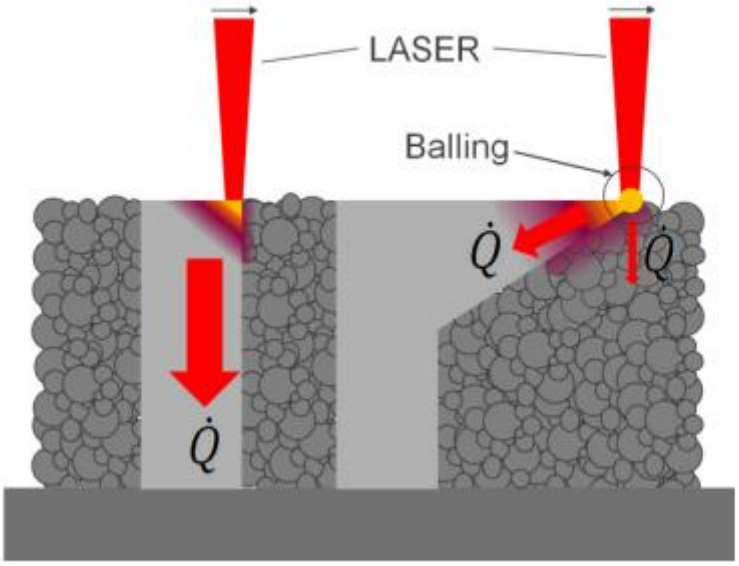

Figure 43 Heat conduction mechanism through the dense solid material and loose powder.[28]

Figure 43 demonstrates the heat conduction's principle during SLM. It can be said that in comparison with the conduction through dense solid melted material, amount of conduction through loose powder is almost negligible. Poor heat conduction may cause a number of problems from balling and gas entrapment to deformation. Therefore, ensuring good heat conduction was one of the main pillars when designing a prop support for mini tensile rods tested for this work.

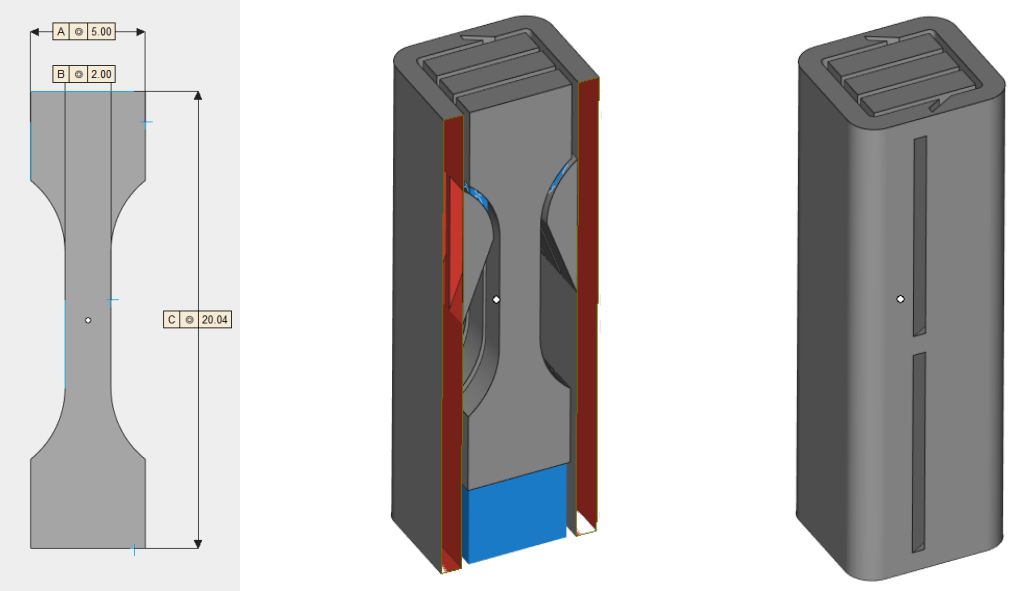

Figure 44 Mini-tensile bars build with the thickness of 1.3 mm and prop supports setup.

Both the first samples explained and mini tensile bars are built and tested for energy input homogenization and flow optimization tools in comparison with default MS1 process.

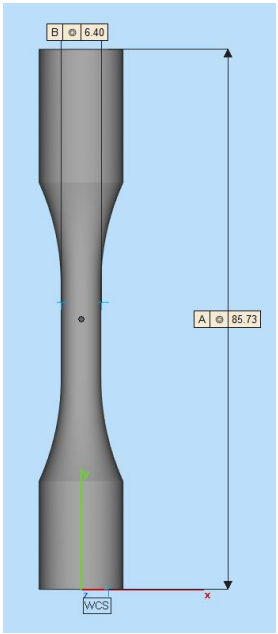

Figure 45 Cyclic testing sample.

Figure 45 shows the fatigue test samples that were printed. The aim of these samples differ from previous ones as energy input homogenization tools are not used for building of these parts. Cyclic testing will be used for observing the effect of potential inner defects that might be formed due to defocusing or scattering of laser beam.

4 Evaluation of Results and Recommendations

In this chapter results of the various tests that has been carried out will be explained and their correlation with OT data will be discussed. In order to observe the changes in microstructure and mechanical properties of parts built depending on the strategies chosen post-process solution treatment or aging treatments were avoided.

4.1 Evaluation with Light Microscope

Top surface of the some of the parts with 5 mm thickness were scanned by optical microscope Alicona IFM 4 which can be used for measurements at µm and sub-µm ranges. This way a closer look at the melting tracks formed by hatching vectors was obtained. It must be kept in mind that measurements on this subchapter will be approximate.

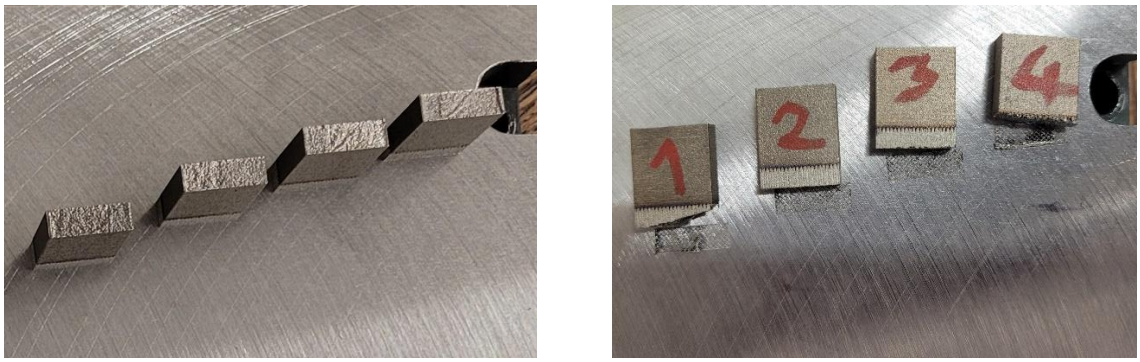

Figure 46 Samples built for the purpose of melt pool track and metallographic inspection.

Part number 1 refers to building by default process while number 2 with time homogenization, 3 with power reduction factor and number 4 is built by using flow optimization.

Working principles of process manipulation tools were explained before and regarded while evaluating the top surface of these parts each mechanism of these tools. Difference in the formation of melting tracks was drastic for default and time homogenized process. According to the process settings the hatch vectors are parallel to each other. At ends of each hatch vector laser does a "U-turn", and continues with exposure of the next vector. However, as it can be seen in Figure 47 A, exposing with default process while laser does the U-turn end of two different melting tracks seem to be solidified together.

In comparison, Figure 47 B demonstrates the melting tracks formed by using time homogenized process. The average length of the melting tracks in this example is 6.3 mm, based on scanning speed of 960 mm/s, it takes 6.5 microseconds for the exposure of one hatch vector. Since time homogenization is set to 10.41 ms, it can be said that in between exposing subsequent hatch vectors, there is 3.91 ms idle time for the laser. It can be seen in the image that melting tracks did not melt and solidified together unlike default process. Based on the difference of 3.91 ms waiting time in between subsequent hatches prevents conjoining of melting tracks. As a result, average melt pool width for default process is approximately 165 µm while it is around 95µm for time homogenized process.

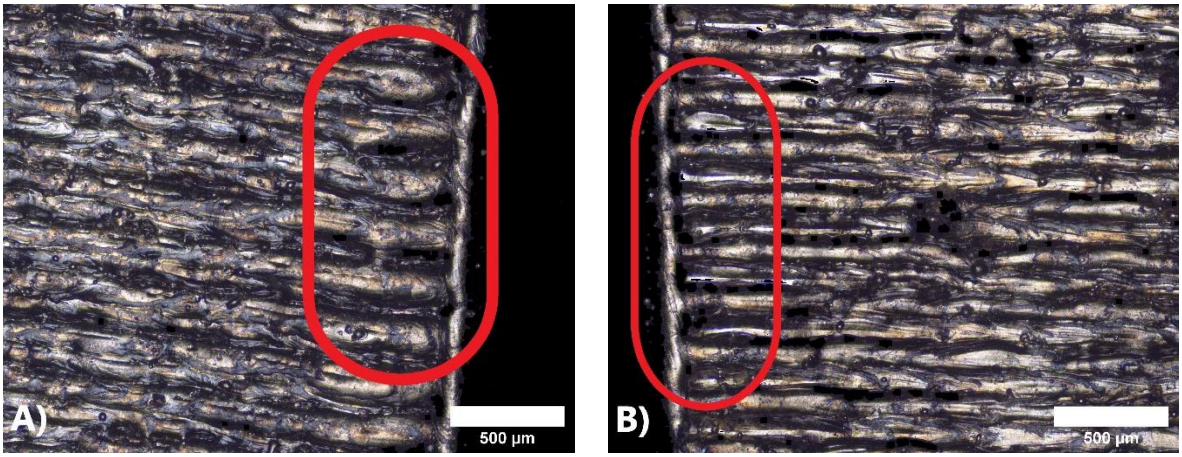

Figure 47 A) ends of melting tracks formed by default process, B) end of melting tracks formed by time homogenized process.

Figure 48 demonstrates another process phenomenon that might have influence on the resulting melting tracks formations. In the first image red arrow refers to inner gas flow direction and orange arrows indicates the stripe directions. Marked areas on the integrated OT image refers to stripes at which melting tracks on Figure 47 were printed. The same amount of heat is applied to the part in a longer time therefore it is expected to see blue-ish(low intensity) signal map on OT. In addition, non-uniform map of OT image also happens when the stripe direction is the same as inert gas flow. Thus, defocusing of laser beam might also be considered as a reason for smaller width of melting tracks by decreasing the heat input.

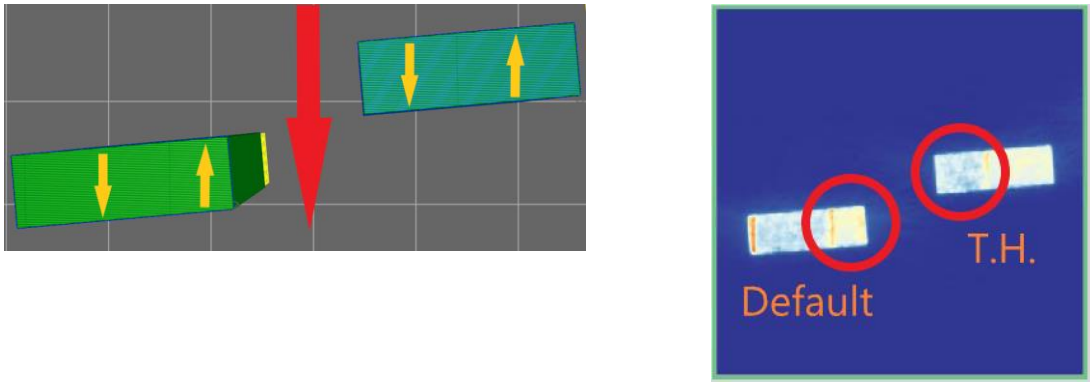

Figure 48 Stripes(Orange), inert gas flow(Red) directions and OT integrated image for default and Time Homogenized process.

Figure 49Figure 48 Stripes(Orange), inert gas flow(Red) directions and OT integrated image for default and Time Homogenized process.

shows examples of melting tracks built by using 20 % power reduction factor. The average hatch vector length of these examples is 4.42 mm. The laser power can be calculated as 253.2 W for these hatch vectors which is 11.2 % reduction in power. The difference such reduction in power results in melting tracks width approximately around 150 µm. According to the Figure 49, it can be said that conjoined tracks seems to have formed similar to the default process setting.

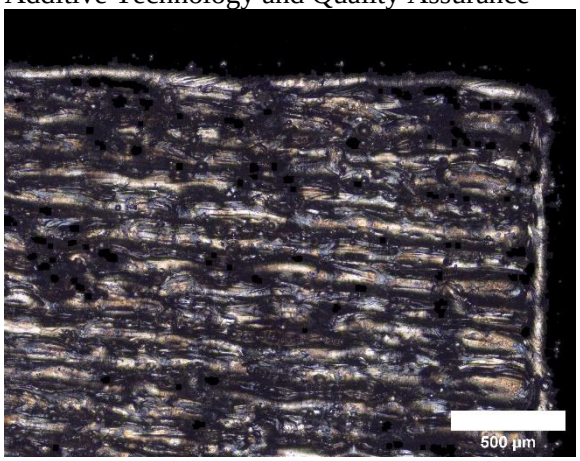

Figure 49 Example of melting tracks built with power reduction factor.

Based on GV curves provided by OT some observations may be done regarding heat input and melt pool formation. Mean GV of each layer throughout the building height is shown in the Figure 50. Firstly, average GV of power reduced process is lower than that of default process which directly correlates with the smaller average melting track width in comparison with the melting tracks built with default process. 11.2 % power reduction on average may be contributing to lower GV curve. Another reason for these results could be due to overlapping zones between melting tracks becoming smaller based on decrease in width of the tracks.

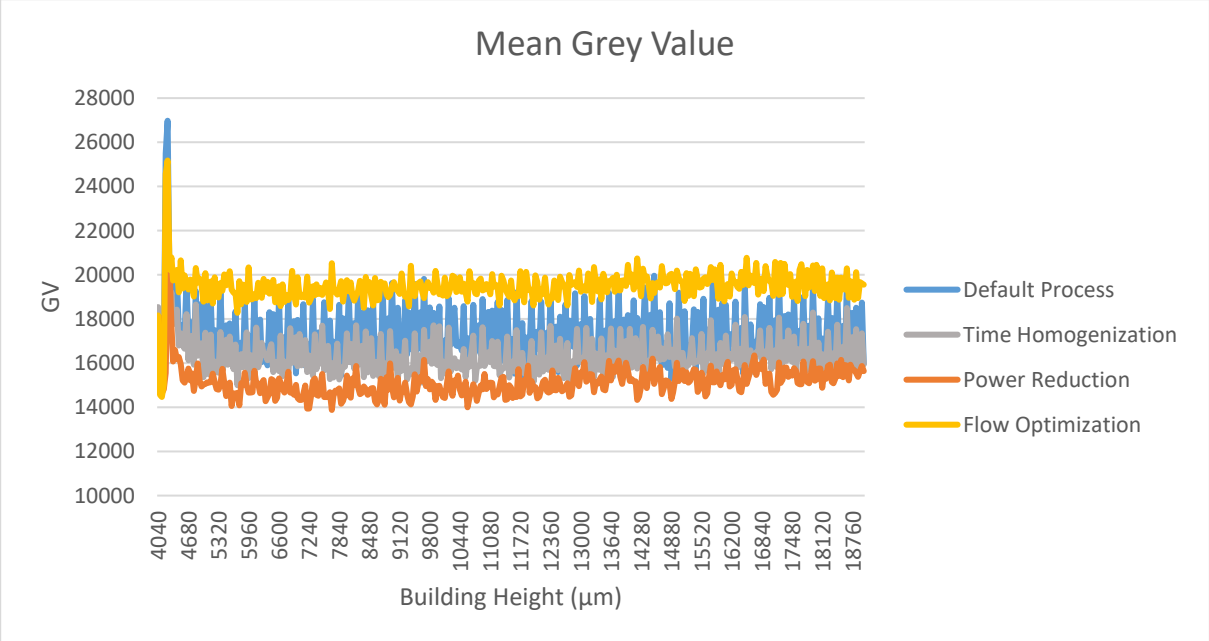

Figure 50 Mean grey value curves of each layer of part built with different methods, based on building height.

Secondly, average of GV curve of time homogenized process is expectedly lower than average of default process. However, it is higher than that of power reduced process although it results in melting tracks narrower in comparison with power reduction. This is perhaps due to higher energy input with time homogenization for each hatch vector while idle time in between exposure of vectors preventing formation of conjoined melting tracks.

Flow optimized process seem to have resulted in greater average of GV curve and lower standard deviation in comparison with other strategies. However, there was not any apparent changes with the default process with regards to melting track formation.

There are many factors affecting the signals recorded by monitoring systems as explained in the previous chapters. Most of those factors were affecting the signals in terms of the changes on conduction rates and heat input. However, there is one more factor that should considered while evaluating OT data. Similar to laser beam defocusing due to smoke and plasma, the radiation emitted from melt pool also interacts with side products of the melt pool. In the case of flow optimization though, these interactions are avoided therefore OT camera is able to gather more direct data coming from melt pool and this results in increase of GV signals. In conclusion it can be said that flow optimization results in both higher energy input and also the melt pool data is gathered more efficiently.

Parts built with SLM contain an inherent anisotropy due to layered production. Nevertheless, application of consistent heat input all along building height of a part might help resulting in one less phenomenon causing incidental anisotropy. When GV of OT evaluated, it is seen that on Figure 51, the functions used in this work relatively help with the randomness of melting process.

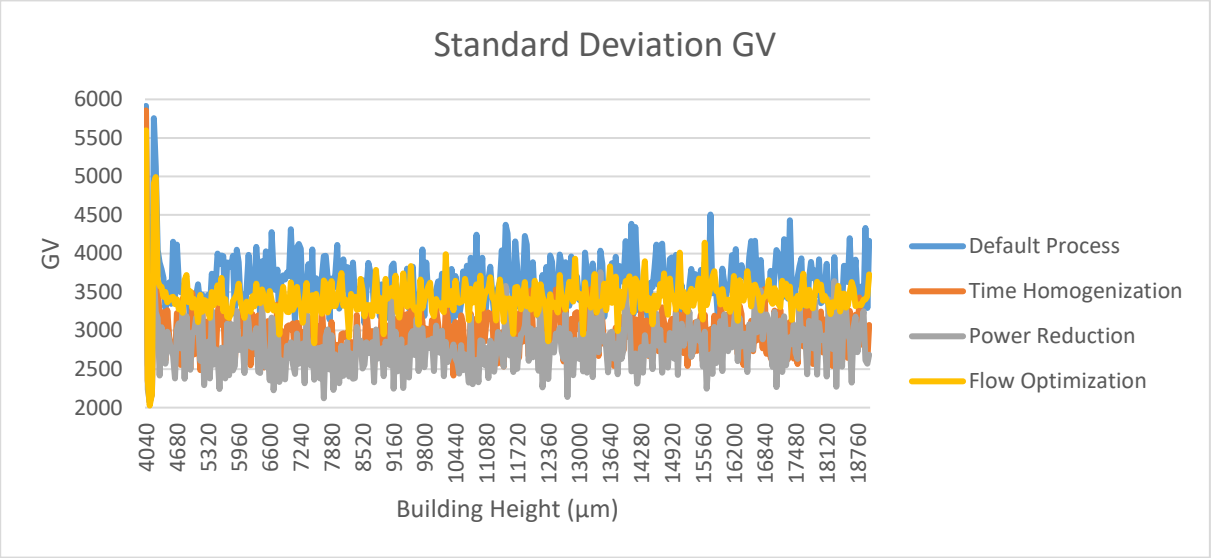

Figure 51 Standard Deviation of grey value curves of each layer of part built with different methods, based on building height.

4.2 Residual Stress

Temperature Gradient Mechanism (TGM) has been explained before as the dynamic behind residual stresses present in the parts which are built with SLM method. TGM explains the formation of residual stresses in terms of expansion and contraction behavior of melted material. Scanning strategies that are tested in this work cause differences in melting mechanism of SLM as it was visible to evaluation by optic microscope. Therefore, it was possible that different scanning strategies may result in different amplitudes of residual stresses within the parts.

Samples designed with 5 mm thickness were also used for this measurement. Hole of 2 mm in diameter and 1 mm depth were drilled. Drilling direction was selected as shown in Figure 42. This was based on the expectation that most of the changes in thermal stresses due to scanning strategies would take place near edges of the parts. And by drilling the parts in this direction deformation released during measurement would correspond to differences in the thermal stresses. In addition, since layer thickness of the process is 40µm, drilling with 2 mm diameter includes large number of layers, which is preferable, to compensate for the randomness of turning and shifting of scanning strategies in between layers.

20 parts were tested as 5 for each default, time homogenized, power reduced and flow optimized processes.

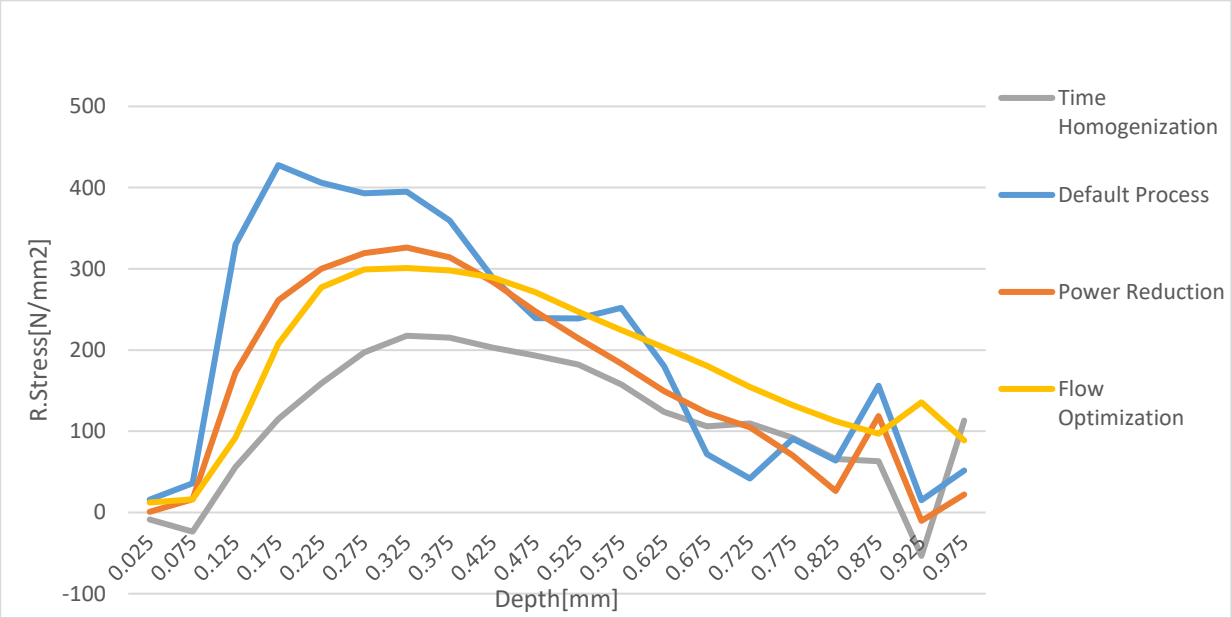

Figure 52 Average residual stress curves depending on drilling depth.

According to the curves on Figure 52, residual stress values seem to have similar trends depending on the drilling depth for all strategies. The peak residual stresses were observed between the drilling depth of 0.125 mm to 0.475 mm. However, regarding amplitude, time homogenization led to biggest drop while power reduction and flow optimization also decreased the residual stresses. The highest residual stress for default process is around 400 N/mm^2, for the case of power reduction and flow optimization it was around 300 N/mm^2 and time homogenization resulted in around 200 N/mm^2.

The results from residual stresses, to a large extent, directly correlate with the melting track formation. Default process results in widest melt track formation and with tracks conjoining at ends of hatch vectors and this process setting result in the highest about of residual stresses. Larger volume of material that is expanding and contracting might be applying more stress to the previously built layers. Time Homogenization results in single melting tracks which are which are much narrower and possibly the reason why for lower residual stresses. Melting track width was approximately 165 µm for default process and 95 µm for time homogenization.

As explained before GV from OT also drops with time homogenization. Therefore, it can be said as the overlapping between the tracks decreases OT signal also drops which could also be

related to the explaining drop in residual stresses. However, as stated before, while evaluating the outcome of OT data, process settings must be regarded and additional evaluation must take place. In the case of this work, drop in OT data, melting track formation and changes in residual stresses seem to relate in a direct manner.

Evaluating the residual stresses that resulted by power reduction in comparison with the other processes, melting track width seems to have an influence here as well. The melting track width was around 150 µm for the power reduced process. Melting track width became narrower in comparison to default process and conjoined melting tracks were still apparent despite the reduced power. The resulting peak residual stresses drops by 25% with power reduction.

Similar to time homogenization, power reduction has also caused the decrease in average GV curve. Power reduction has led to larger drop in GV while time homogenization resulted in larger drop on residual stresses. A possible mechanism for these results can be rooted in the relation of OT values with the melt pool depth.

So far melting track width in relation with GV values was discussed to explain possible connection with the residual stresses. But as melting is taking place on a 3- dimensional manner, melt pool depth also dictates the volume of material that is being melt. For this reason, not only top surface of the parts but also the side surface, that is selected for testing, was scanned with optic microscope as well. However, due to the fact that heat is applied to every layer by shifting and turning the scanning strategy in between, the results of this scan were difficult to evaluate for the purpose of observing melt pool depth. Moreover, since scanning strategies used for this work specifically affect the short hatch vector, it means that there were variations even within the same layer. Based on this reason it is impossible to draw conclusions on the melt pool depth based on the experiments done. Figure 53 demonstrates the complexity and variety in between melting tracks.

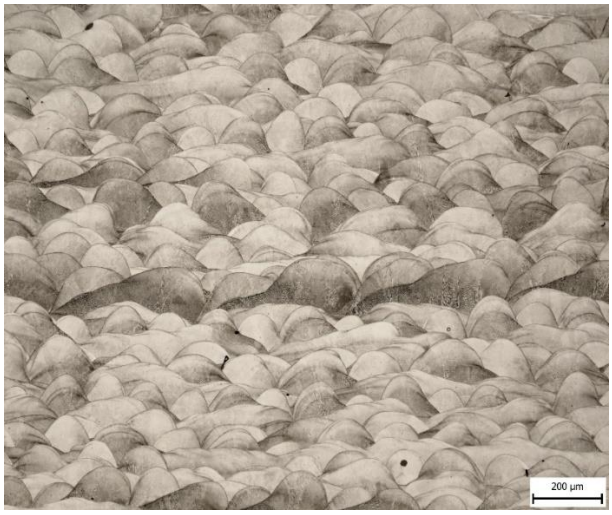

Figure 53 Melting tracks formed scanned by optic microscope after 3 % nital etching and 100x zoom in.

According to the Figure 50, flow optimization had the highest average GV curve. However, it resulted in lower amount of residual stresses. These results point out the complexity of the process regarding residual stress formation and how difficult it is to draw conclusions based solely on OT data. A possible reasoning for the decrease in residual stress by flow optimized process might be laying in the stress relief taking place during process. Due to continuously

higher energy input by this manipulation too, it might be possible that heat affected zone of parts along building height can be longer or its average temperature might be higher thus leading to relief of residual stresses.

4.3 Micro-hardness

SLM process includes very high cooling rates that greatly influence mechanical properties of parts. Scanning strategies that are tested for this work influence the melting and solidification behaviors as discussed before. Therefore, it plausible to expect changes in cooling rates as well. Differences in hardness are investigated as a result of various cooling rates in relation with microstructure.

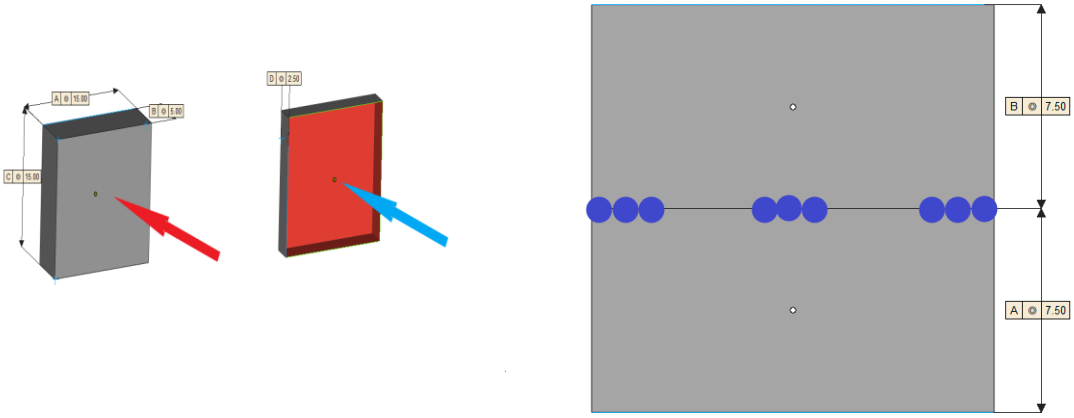

Figure 54 Micro-hardness is measured at the points marked both on surface and core of the parts after removing half of the thickness.

As mentioned before, the scanning strategies tested for this work are based on generally manipulating the parts near edges of layers as that is where short hatchings take place. Measurement of microhardness was planned for evaluation at the surface of the parts as well as at the "core" of the parts. In addition to that, with regards to variety of scanning strategies on each layer, three different locations were selected for the measurement on each surface. After surface was done 2.5 mm of material was removed and the same measurements were repeated on the new surface. This procedure was done on four parts built with different strategies.

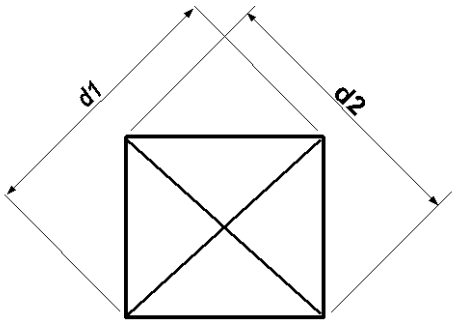

Figure 55 Vickers hardness test indentation type.

Vicker's hardness measurement was used. The load was 10 kg and the goal was to have the diagonal length of the indentation (d1 and d2, Figure 55) to be bigger than 200 µm. Since the layer height for this work was always 40 µm, by obtaining such indentation size was aimed to contain multiple layers in the measurement.

Table 3 Microhardness testing results for different strategies

Part	Core Hardness(HV)	Surface Hardness(HV)
Default	393	364
Time Homogenized	390	368
Power Reduced	390	359
Flow Optimized	392	365

Results of microhardness testing is given on table 3. Even though, 9 measurements were done on each surface, there was no significant change in the results regardless of location on the surface. Therefore, results shown here are average of 9 measurements on each surface.

One of the common points in between the results of different scanning strategies was that core of parts always seem to have higher hardness than that of surfaces and the difference was always approximately 10 %. There were not any significant changes found based on different scanning strategies.

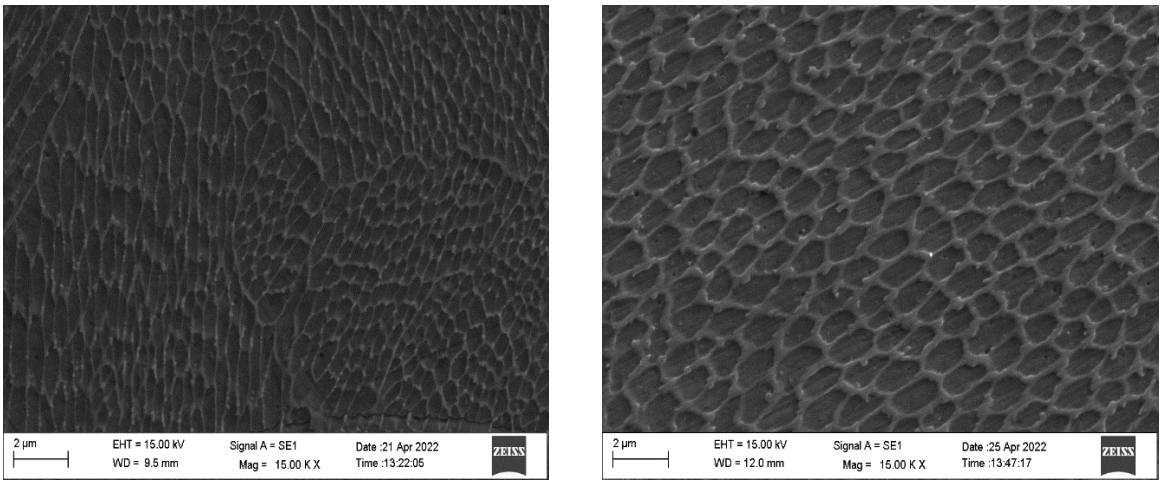

Figure 56 Scanning Electron Microscope (SEM) images of core and surface of parts built with default process.

The locations on which the hardness was measured, were also scanned by electron microscope. This way, observation of the microstructure and its properties in regards to results of hardness was aimed.

Figure 56, shows the pictures taken from the part built with default process. First picture is from the core while the second one was taken by scanning the surface of the part. While it is difficult

to quantify the differences in microstructure based on the images there are a couple of visible differences. In the first picture the average grain size is relatively smaller than that of second image. This could be attributed to higher cooling rates at the core of the part in comparison to the surface of the parts. One of the reasons for this could be related to the fact that loose powder around the parts while SLM process acts similar to isolation that might result in lower cooling rates which leads to grain coarsening that is seen in the second image.

Another difference to point out in the pictures is the precipitations forming in the second image. Precipitates are also coarser on the surface image and more visible at the borders of grains. This could be another sign of lower cooling rate on the surface of the part that gives chance to precipitates squeezing coarsening and squeezing into the grain boundaries.

Another possible reasoning for the higher hardness value measured in the cores of the parts could be related to the difference in the heat input differences between the core and surface of parts.

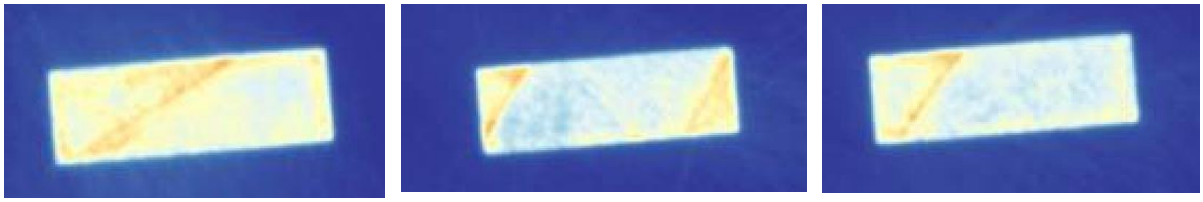

Figure 57 OT integrated images from the multiple layers of the part built with default process.

A subjective look into OT integrated images based on multiple layers of the part built with default process is shown in Figure 57. At first glance, there seems to be a pattern repeated in many layers. Due to short hatchings higher intensity(red-ish) zones on each part indicates higher energy input near the edges of the parts. In addition to cooling rates heat input might also be included in the resulting higher hardness at the core of the part. However, a more thorough evaluation is necessary as scanning strategy tools do change the heat input near edges of the parts while in terms of hardness there was no significant difference.

4.4 Tensile Testing

GV curves for part with different geometries and variations in heat input in regards to part with different cross sections were explained briefly on chapter 3.2 Design of Experiment. In this chapter a closer look is taken for building mini-tensile bars and resulting GV curves. As mentioned before, one of the main mechanisms drastically influencing the resulting GV curve is ratio of the heat input and conduction rate.

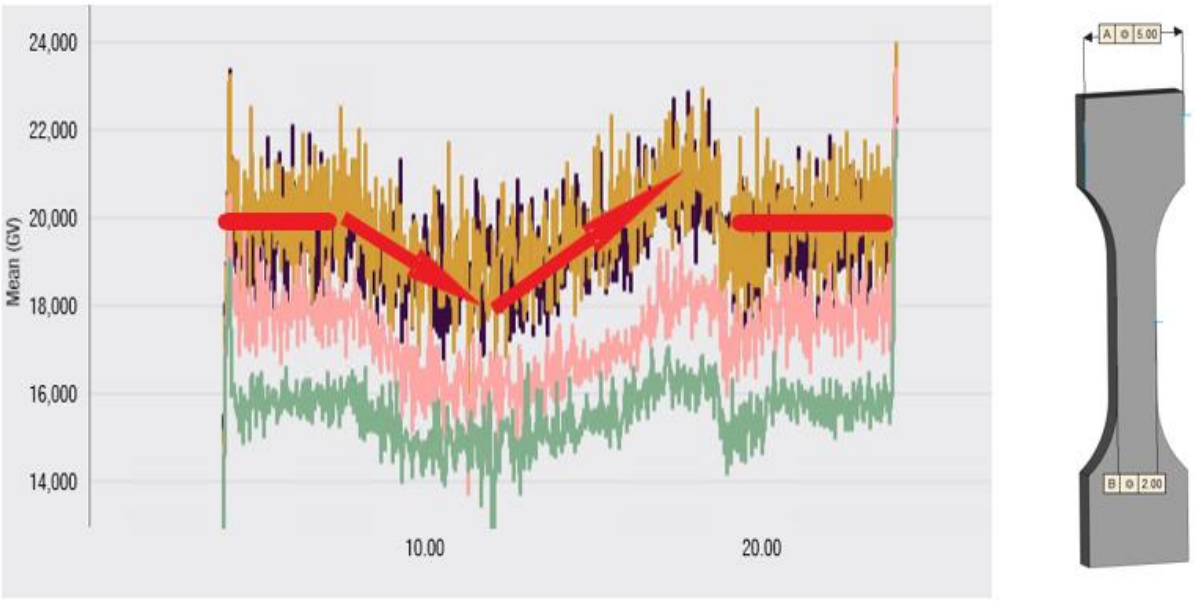

Figure 58 GV curves for parts built with different scanning strategies along with building height and mini tensile bar samples.

While building mini-tensile specimens, pattern that can be seen here in the Figure 58, was repeated regardless of the strategy that is used for this work. Dropping trend was observed when the cross section of the part becomes smaller as ratio of heat input to conduction decreases. However, during building gauge length of the parts, there is trend of increasing GV. This is due to conduction rate decreasing as building height increases. As it is seen in the figure, average of flow optimized process(Yellow) and default process(Black) were similar, as time homogenized(Pink) process resulted in lover GV and power reduced(Green) the lowest.

The smallest cross section of these parts was as explained before 2x1.3 mm and as it can be seen on Figure 59. Such cross section dictates the application of the scanning strategies. Hatch vector length is limited by the cross section. For such a small cross section, while it is difficult to calculate an average length of hatch vectors. For the approximate estimation of idle time between exposure of hatch vectors and reduced power that will be utilized, average hatch vector length will be assumed as 1.5 mm. And calculations will be done similar to the chapter 4.1 Evaluation with Light Microscope. So, the time necessary is calculated by dividing the hatch vector length with the scanning speed of 965 mm/s. Thus, for exposure of one hatch vector, the necessary time period is 1.5 ms. And to calculate idle time in between exposure of hatch vectors, 1.5 ms is subtracted from the minimum vector time of 10.41 ms, therefore idle time during exposure of these parts is 8.91 ms. In addition, since the average presumed vector length is 1.5 mm and the general stripe width is 10 mm. The reduction in the power will be 17 %. Therefore, the average power setting used for the exposure of a cross section of a part will be 250.8 W.

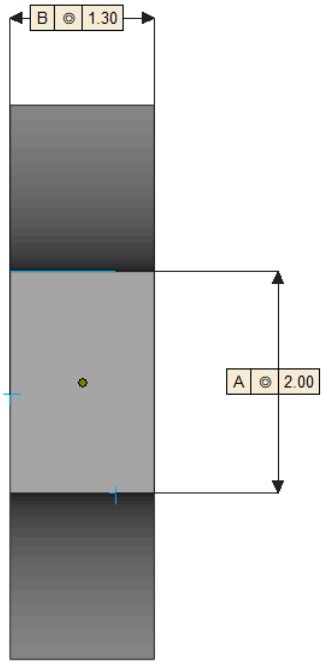

Figure 59 Testing cross section of mini tensile bars.

This part design was selected for the tensile testing for purposefully obtaining an experiment that susceptible for the changes in scanning strategies. And according to the OT data, as the parts' cross section becomes smaller the gap between the amplitude of data obtained for different scanning strategies becomes larger. This is due to majority of hatch vector while exposing a layer becoming short hatches.

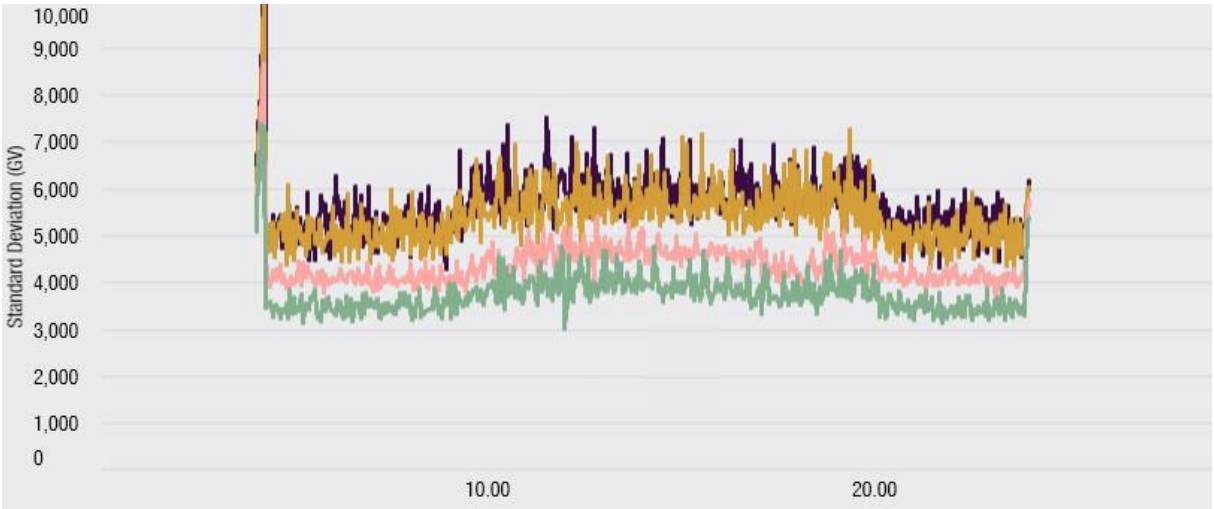

Figure 60 Curves of Standard deviation of grey values for parts built with different scanning strategies along with building height and mini tensile bar samples.

Figure 60 demonstrates the standard deviation of the tensile bars. Similar to the Mean GV curves, power reduction resulted in lowest mean values while flow optimization and default process resulted in similar standard deviations.

Unexpectedly, there were not any major differences in the results of tensile testing except for elongation at maximum force(A_g). Mechanical properties such as offset yield strength($R_{p0.2}$), tensile strength(R_m) and elongation at break (A_5) showed no significant difference. Elongation at maximum force was found to be 2.25 % for default process, 2.31 % for time homogenized parts, 1.74 % for reduced power and 1.59 % for flow optimized process. Therefore, it showed no significant difference between time homogenization and default process. However, both power reduction and flow optimization resulted in lower elongation at maximum force. For which there were not any signs by OT.

Unfortunately, there was no correlation between these results and OT data. Since the part designs are identical for every part and the part orientation were near identical inside building chamber, therefore it can be assumed that parts were subjected to the same heat transfer rates. Based on this assumption, changes in the performance of the parts were expected as the heat input is different. But unexpectedly to a big extend parts performed similarly. Nevertheless, the amount of anisotropy that these parts contain can be expected to drop in accordance with the lower standard deviation of the data provided by OT. Which means parts built with time homogenized process and power reduced process can be expected to have less amount of anisotropy.

4.5 Fatigue Testing

Fatigue testing regarding scanning strategies was carried out to evaluate possible results of using flow optimization. Irregularities in the inert gas flow was deemed more likely to cause inner defects such as lack of fusion and balling. Therefore, cyclic loading tests were applied to the part built with default process parameters and flow optimized process.

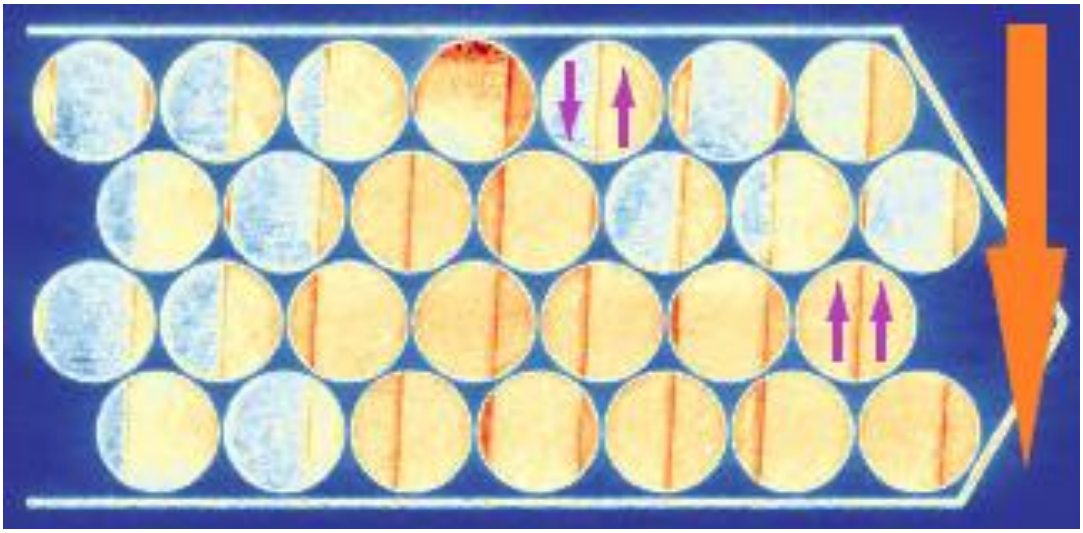

Figure 61 Cross section of the experiment design for cyclic testing rods and arrows indicating directions of stripes(Purple) and direction of the inert gas flow(Orange).

Laser beam's interaction with the smoke and plasma that ascends over melt pool has been discussed before. Figure 61, gives a view on distinctive difference of such phenomenon's result in the light irradiated from the melt pool and its fraction that reaches the CMOS censor. The importance of this view is distinguishing non-uniformity in heat input caused by de-focused or scattered laser beam. As it can be seen in the figure, when the direction of a stripe(purple arrow)

is along with the direction of the gas flow(orange arrow), the pattern of non-uniform, low intensity arises. While the stripe direction is against the inner gas flow however, the results becomes relatively more uniform higher intensity signal. As explained before this is due to both higher energy input by flow optimization and higher amount of near-infrared radiation captured by CMOS censor.

Potentially lower energy input by scattered laser beam has higher tendency to result in inner defects. Based on this, cyclic testing results and OT data will be compared to find relations between this process mechanism of lower energy input and defect formation.

However, there are a few drawbacks of using a system such as OT. As discussed before OT data should always be evaluated while regarding the process settings and possible phenomena that might be causing instabilities during process. OT data cannot be the sole base for drawing conclusions. As it was shown before both higher and lower average GV in comparison with default process, might lead to lower residual stresses. Therefore, the effect of multiple phenomena taking place simultaneously should be considered.

In addition to that, the resolution of the OT camera is 145 µm per pixel. Which means it would be rather difficult to detect individual defects within the parts that are smaller than the resolution of the camera.

Due to the reasons explained, a different approach for evaluating the OT data was necessary. Instead of micro evaluation of individual errors within parts, in this work a macro evaluation of the process will be attempted.

There are a maximum and integrated value image generated by OT for every layer of each print job. In order to detect formation of a defect, any instability on a OT image must be noticed by an engineer and the previous or next 3-5 layers should be checked, in order to examine the re-occurrence of the instability. This is due to the fact that laser is powerful enough to re-melt 3-5 layer during exposure. Since there can be a huge number layer to be observed, it makes observation of inner defect by OT difficult.

On the other hand, it must be mentioned that OT does have algorithms for defect evaluation that could point out the effects of defects. But calibrating such algorithms rely on a lot of data gathered by building identical prints regularly and evaluating the part built with material testing.

Macro evaluation mentioned will be focusing on general trends within a SLM print. While doing so, the goal is not to identify effects of individual defects. But to point out the more likely parts of samples built, that might contain defects. The advantage of this approach is that it requires less amount of data thus it is more flexible tool to be used with different prints.

An example of this approach is given on Figure 62. First image is obtained by stacking the images that are generated by OT. Later on intensity threshold on Fiji(Imagej) software was used by focusing on higher intensity signals recorded. The higher the threshold is the less of the lower intensity fields are removed. Supports are built with lower energy intensity. As threshold is increased supports are removed as well and thresholding can be continued until high energy density points on a part can be viewed. The same approach can be used for lower intensity points as well.

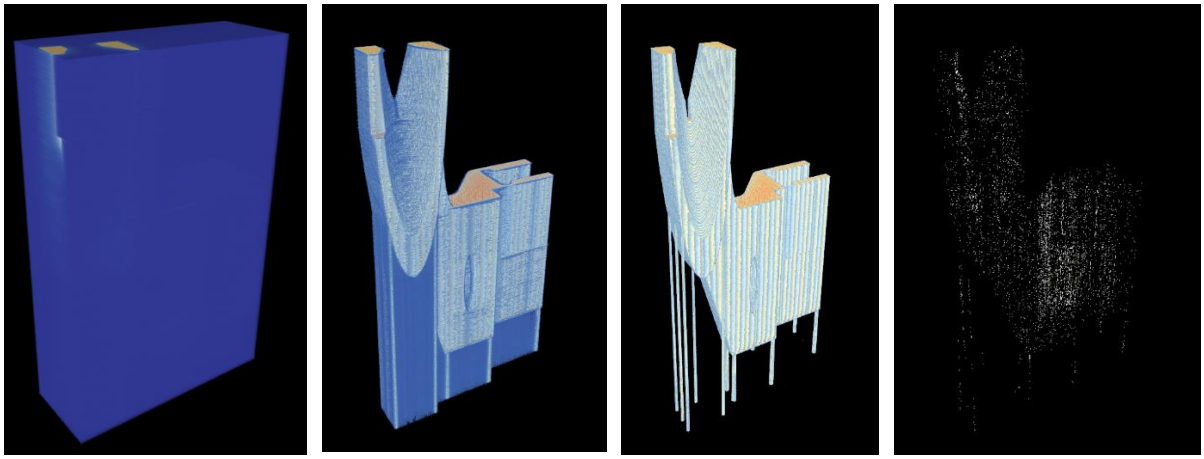

Figure 62 An example of 3D evaluation focusing on high intensity signals.

For the purpose stacking images to create a 3D view, images of each layer are necessary. To export the images of a part from OT a script was programmed by using Python language. By this script, area of interest on a layer can be marked and image of this area can be exported while going through each layer automatically. The script can be adjusted for each part and each area of interest on a layer and the amount of layers to be observed can be selected as well. Cyclic load testing for this work was focused on the influence of scattered laser beam, thus while evaluating the OT data, problems that might arise due to lower energy input was the main interest.

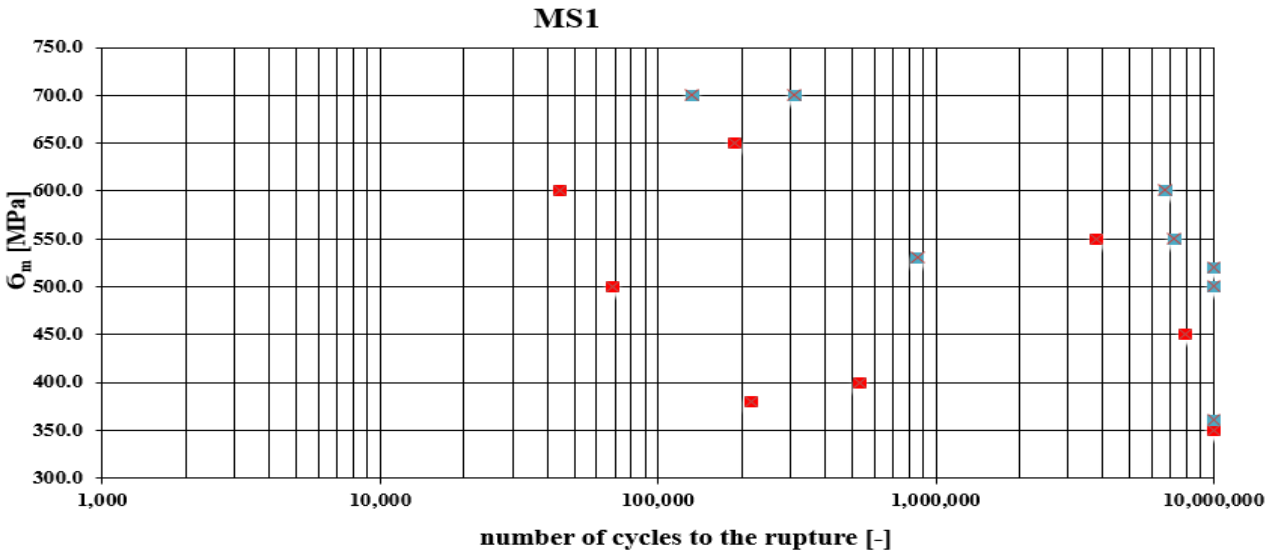

Figure 63 Fatigue testing results of parts built with and without using flow optimization.

Figure 63 shows the results of the cyclic testing results. These tests were run with R=0.1 ratio, which refers to the ratio of minimum peak stress and maximum peak stress that parts have undergone. Blue dots on the graph indicate the results of testing of the parts that were built by using flow optimization. And red dots indicate the results of default process settings. Flow optimized parts were capable of reaching $10x10^6$ cycles under various loads while non-

optimized parts performed poorly in comparison. Based on this result, it can be said that there is clear adverse affect of laser scattering that is causing parts to rupture at lower amount of cycles under various loads. For evaluation of these parts through OT, the script was adjusted for exporting images that would involve 4 of the parts. Two of the parts evaluated are built with flow optimization and 2 were built using default process. Sum of gauge length of the cyclic testing rods and radius of these parts were the area of interest. Therefore, script was also adjusted only to involve only a portion of these parts that is as long as 51 mm.

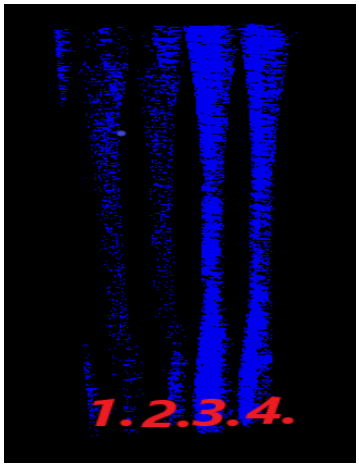

Figure 64 3D view of low intensity(cold) spots of parts, 1. and 2. flow optimized process and 3. and 4. default.

For the purpose of observing frequency of cold spots formed on OT integrated image, the thresholding was done on only blue channel of the stack of the pictures. Since blue spots point out potential locations for the effect of defects such as lack of fusion and balling. The significantly bigger amount of blue spots seen on part built with default process, directly correlates with the poor performance of the parts under cyclic loading.

Figure 65 An example for 3D view of high intensity(hot) spots of a part built with flow optimization and broken part after testing.

Figure 66 Another example for 3D view of high intensity(hot) spots of a part built with default settings and broken part after testing.

Although the data was evaluated for cold spots it correlates with the results of cyclic testing, the data from OT was also filtered to focus on high intensity(hot) spots. Figure 65 and Figure 66, demonstrate the examples of hot spots in comparison with actual fracture under cyclic loading. Similar to cold spots, hot spots are also more common in part built with default process. This might indicate higher frequency of the defects that could be formed due to over heating of the parts. Which would mean non-flow optimized process may also result in defects like gas entrapment or deformations. However, the OT results for hot spots were not repeatable for every part. Therefore, there might be a phenomenon other that scattering of the laser that might result in potential hot spots.

5 Conclusion

The general scope of this work was to observe and investigate some of the phenomena that take place during the Selective Laser Melting process. The SLM process is very complex and its premise is near limitless geometrical freedom during manufacturing. In order to better explain the workings of this process, the Optical Tomography monitoring system was utilized, and several strategies were tested with respect to mechanical properties and monitoring data.

In the research section of this work, the SLM process was explained. The fundamentals of working principles of the process starting from the data preparation was generally discussed. The form of the materials used, were discussed with respect to important aspects of their compatibility with the process. The process parameters were explained and some of the examples of the application of heat energy in relation with process parameters were shown. Later on, thermal phenomena and defect formation during SLM process were discussed in relation with the aim of this work.

In the second section of this research, some monitoring system examples and their utilization in the scientific literature were discussed. Several different setups and approaches were explained. Some of the devices based on their working principles of their sensors and the evaluation of their outputs were explained. Examples of utilization of such devices with respect to setups in which they exploited, were given. The goal in this part of the research was to investigate the possible usage of monitoring systems in order to lay the ground knowledge for explaining the working principles of monitoring system that is utilized in this work.

One of the main goals of this work was to obtain a better understanding of the SLM process. While aspiring for that, the experiments were also designed to test the utility of some of the most used SLM process adjusting tools in RTI. Flow optimization, Time Homogenization and Power Reduction were selected for that reason. This way, the variety of the processes would be provided by these tools, and the evaluation of their effect on the final properties would be investigated by the help of the Optical Tomography system.

For the purpose of comprehensive evaluation of the potential changes that might be caused by the tools tested on this work, series of experiments and evaluations were carried out. Since the melting behavior has substantial influence on final properties of built parts, several parts were designed and printed to be scanned by light microscope. Significant differences were discovered between the formation of melting tracks during the SLM process. The default process settings resulted in conjoining of subsequent melting tracks, at very ends of them, and creating widest melting tracks. Secondly, Time homogenization led to avoiding conjoined tracks and width of melting tracks were near half of the ones built with default process. Power reduction also caused melting tracks to have narrower widths while still forming conjoined tracks. And all these were correlating with the OT data. The higher the Grey Value recorded by OT, the wider the melting tracks became. On the other hand, narrower melting tracks and less overlapping between tracks resulted in lower GV recorded. The OT values did not show any significant change between the flow optimized process and the default process settings. There was no significant change in the melting track formation.

The residual stress measurements were evaluated based on the expectation that larger amount of melted material per unit time would result in larger residual stresses. And residual stress testing was one of the tests that correlated with melt pool formation and OT data to a large extend. But flow optimization was again different than general trend of results. According to the residual stress measurement results, narrower melt pool tracks resulted, generally, in lower OT values and lower residual stresses. Since power reduction has resulted in narrower melting tracks and also decreased residual stress in parts. For the case of time homogenization, narrow, separate tracks resulted in much lower residual stress in comparison with default process. So far, both residual stresses and melting track formation correlated well with the OT data. Although, while the flow optimization resulted in higher GV output, it resulted in lower residual stresses in comparison with the default process. A theory for this result could be the stress relief that is caused by a higher energy input due to the flow optimization, but there was not sufficient data to support this idea.

In the next sub-chapter another performed test is described. The purpose was to observe micro-hardness of the parts built. Since, differences caused by different scanning strategies were expected to take place near edges of the parts, micro-hardness was measured both on surface and core of the parts for comparison. Interesting result was the fact that core of the parts had 10% higher hardness than that of surface, regardless of the process settings. Since OT had provided different amplitudes of data for each process and hardness was relatively the same, it

can be said that differences in OT data did not correlate with the results. When microstructure was observed, there was a visible difference in the surface and core of part built with default process, relative grain coarsening and precipitation was apparent. And according to the OT integrated image, near the edges of the part, was subjected to the heat for longer period of time. These two results may indicate both higher energy input and lower heat transfer rates at the surface of parts. However, since there were no significant differences in the results for different scanning strategies, further investigation is necessary.

The mini-tensile tests were also carried out. It was found that, as expected, the smaller the cross section of a part, the bigger are the changes between the data obtained from different scanning strategies. Although, there were not significant changes in the mechanical properties of the parts built. Due to the common aspect of very small cross section areas micro-hardness and mini tensile may potentially point out shortcoming of OT system.

The last tests that were discussed in this work was the cyclic-fatigue testing. The expectation was that phenomenon that scattered laser beam could result in higher amount of inner defects. These tests were selected to be done only on the specimens printed using the default and the flow optimized process. According to the OT data, the effect of scattered laser beam and lower energy input was obvious by monitoring. And in addition, a python script was developed for automation of data evaluation and it was tested by comparison with fatigue test results. This evaluation method resulted in direct correlation with fatigue results. More amount of low intensity or cold points found in OT data by automatic evaluation resulted in rupture at lower amount of cycles. The differences in OT data were visible between default and flow optimized process. However, when tested for high intensity or hot spots, the OT results only correlated with rupture of some of the parts. Therefore, further investigation and/or further development in the python script is necessary.

There were some important outcomes of this work. Above all, for melt pool formation, residual stress and fatigue testing OT data showed direct correlation. On the other hand, micro-hardness and mini tensile testing did not result in similar correlation with the OT data. Finally, the OT data should be evaluated with respect to the process settings and testing results. The OT data cannot be a sole base or evidence for understanding the process instabilities. It can be said that the OT offers a great potential for the process understanding and a possibly wider adaptation of SLM process, while further investigation in many areas of this process is still necessary.

Bibliography

[1] G. T. Gray *et al.*, "Structure/property (constitutive and spallation response) of additively manufactured 316L stainless steel," *Acta Mater.*, vol. 138, pp. 140–149, Oct. 2017, doi: 10.1016/j.actamat.2017.07.045.

[2] V. Petrovic, J. Vicente Haro Gonzalez, O. Jordá Ferrando, J. Delgado Gordillo, J. Ramón Blasco Puchades, and L. Portolés Griñan, "Additive layered manufacturing: sectors of industrial application shown through case studies," *Int. J. Prod. Res.*, vol. 49, no. 4, pp. 1061–1079, Feb. 2011, doi: 10.1080/00207540903479786.

[3] S. Bremen, W. Meiners, and A. Diatlov, "Selective Laser Melting," *Laser Tech. J.*, vol. 9, no. 2, pp. 33–38, Apr. 2012, doi: 10.1002/latj.201290018.

[4] M. Van Elsen, "Complexity of selective laser melting: a new optimisation approach," 2007. Accessed: May 16, 2022. [Online]. Available: https://lirias.kuleuven.be/retrieve/67187

[5] H. Gong, K. Rafi, H. Gu, T. Starr, and B. Stucker, "Analysis of defect generation in Ti–6Al–4V parts made using powder bed fusion additive manufacturing processes," *Addit. Manuf.*, vol. 1–4, pp. 87–98, Oct. 2014, doi: 10.1016/j.addma.2014.08.002.

[6] "SLM Support Design Tampere, Finland Mikko Savolainen, Petteri Kokkonen, Erin Komi - PDF Free Download." https://docplayer.net/129928889-Slm-support-design-tampere-finland-mikko-savolainen-petteri-kokkonen-erin-komi.html (accessed May 24, 2022).

[7] U. Scipioni Bertoli, A. J. Wolfer, M. J. Matthews, J.-P. R. Delplanque, and J. M. Schoenung, "On the limitations of Volumetric Energy Density as a design parameter for Selective Laser Melting," *Mater. Des.*, vol. 113, pp. 331–340, Jan. 2017, doi: 10.1016/j.matdes.2016.10.037.

[8] A. Souza, K. Al-Rubaie, S. Marques, B. Zluhan, and E. Santos, "Effect of laser speed, layer thickness, and part position on the mechanical properties of maraging 300 parts manufactured by selective laser melting," *Mater. Sci. Eng. A*, vol. 767, p. 138425, Sep. 2019, doi: 10.1016/j.msea.2019.138425.

[9] J. Mutua, S. Nakata, T. Onda, and Z.-C. Chen, "Optimization of selective laser melting parameters and influence of post heat treatment on microstructure and mechanical properties of maraging steel," *Mater. Des.*, vol. 139, pp. 486–497, Feb. 2018, doi: 10.1016/j.matdes.2017.11.042.

[10] X. Kan, Y. Yin, D. Yang, W. Li, and J. Sun, "Micro pool characteristics of 316L and the influence of sulfur during SLM," *Opt. Laser Technol.*, vol. 142, p. 107136, Oct. 2021, doi: 10.1016/j.optlastec.2021.107136.

[11] L. Thijs, F. Verhaeghe, T. Craeghs, J. V. Humbeeck, and J.-P. Kruth, "A study of the microstructural evolution during selective laser melting of Ti–6Al–4V," *Acta Mater.*, vol. 58, no. 9, pp. 3303–3312, May 2010, doi: 10.1016/j.actamat.2010.02.004.

[12] M. Guo, D. Gu, L. Xi, L. Du, H. Zhang, and J. Zhang, "Formation of scanning tracks during Selective Laser Melting (SLM) of pure tungsten powder: Morphology, geometric features and forming mechanisms," *Int. J. Refract. Met. Hard Mater.*, vol. 79, pp. 37–46, Feb. 2019, doi: 10.1016/j.ijrmhm.2018.11.003.

[13] H. Yang, J. Yang, W. Huang, Z. Wang, and X. Zeng, "The printability, microstructure, crystallographic features and microhardness of selective laser melted Inconel 718 thin wall," *Mater. Des.*, vol. 156, Jul. 2018, doi: 10.1016/j.matdes.2018.07.007.

[14] W. E. King *et al.*, "Observation of keyhole-mode laser melting in laser powder-bed fusion additive manufacturing," *J. Mater. Process. Technol.*, vol. 214, no. 12, pp. 2915–2925, Dec. 2014, doi: 10.1016/j.jmatprotec.2014.06.005.

[15] P. Tan, R. Kiran, and K. Zhou, "Effects of sub-atmospheric pressure on keyhole dynamics and porosity in products fabricated by selective laser melting," *J. Manuf. Process.*, vol. 64, pp. 816–827, Apr. 2021, doi: 10.1016/j.jmapro.2021.01.058.

[16] Z. Zhao *et al.*, "Influence of pore defects on the mechanical property and corrosion behavior of SLM 18Ni300 maraging steel," *Mater. Charact.*, vol. 182, p. 111514, Dec. 2021, doi: 10.1016/j.matchar.2021.111514.

[17] S. Tammas-Williams, H. Zhao, F. Léonard, F. Derguti, I. Todd, and P. B. Prangnell, "XCT analysis of the influence of melt strategies on defect population in Ti–6Al–4V components manufactured by Selective Electron Beam Melting," *Mater. Charact.*, vol. 102, pp. 47–61, Apr. 2015, doi: 10.1016/j.matchar.2015.02.008.

[18] R. Li, J. Liu, Y. Shi, L. Wang, and W. Jiang, "Balling behavior of stainless steel and nickel powder during selective laser melting process," *Int. J. Adv. Manuf. Technol.*, vol. 59, no. 9, pp. 1025–1035, Apr. 2012, doi: 10.1007/s00170-011-3566-1.

[19] H. Niu and I. Chang, "Instability of scan tracks of selective laser sintering of high speed steel powder," 1999, doi: 10.1016/S1359-6462(99)00276-6.

[20] H. Chen, Y. Zhang, A. Giam, and W. Yan, "Experimental and computational study on thermal and fluid behaviours of powder layer during selective laser melting additive manufacturing," *Addit. Manuf.*, vol. 52, p. 102645, Apr. 2022, doi: 10.1016/j.addma.2022.102645.

[21] D. Wang *et al.*, "Influence of spatter particles contamination on densification behavior and tensile properties of CoCrW manufactured by selective laser melting," *Opt. Laser Technol.*, vol. 121, p. 105678, Jan. 2020, doi: 10.1016/j.optlastec.2019.105678.

[22] A. B. Anwar, I. H. Ibrahim, and Q.-C. Pham, "Spatter transport by inert gas flow in selective laser melting: A simulation study," *Powder Technol.*, vol. 352, pp. 103–116, Jun. 2019, doi: 10.1016/j.powtec.2019.04.044.

[23] P. Mercelis and J. Kruth, "Residual stresses in selective laser sintering and selective laser melting," *Rapid Prototyp. J.*, vol. 12, no. 5, pp. 254–265, Jan. 2006, doi: 10.1108/13552540610707013.

[24] M. F. Zaeh and G. Branner, "Investigations on residual stresses and deformations in selective laser melting," *Prod. Eng.*, vol. 4, no. 1, pp. 35–45, Feb. 2010, doi: 10.1007/s11740-009-0192-y.

[25] S. Clijsters, T. Craeghs, S. Buls, K. Kempen, and J.-P. Kruth, "In situ quality control of the selective laser melting process using a high-speed, real-time melt pool monitoring system," *Int. J. Adv. Manuf. Technol.*, vol. 75, no. 5, pp. 1089–1101, Nov. 2014, doi: 10.1007/s00170-014-6214-8.

[26] S. Berumen, F. Bechmann, S. Lindner, J.-P. Kruth, and T. Craeghs, "Quality control of laser- and powder bed-based Additive Manufacturing (AM) technologies," *Phys. Procedia*, vol. 5, pp. 617–622, Jan. 2010, doi: 10.1016/j.phpro.2010.08.089.

[27] T. Craeghs, S. Clijsters, Jean.-P. Kruth, F. Bechmann, and Marie.-C. Ebert, "Detection of Process Failures in Layerwise Laser Melting with Optical Process Monitoring," *Phys. Procedia*, vol. 39, pp. 753–759, Jan. 2012, doi: 10.1016/j.phpro.2012.10.097.

[28] S. Kleszczynski, J. zur Jacobsmühlen, J. Sehrt, and G. Witt, *Error detection in laser beam melting systems by high resolution imaging*. 2012, p. 987.

[29] T. Craeghs, S. Clijsters, E. Yasa, and J.-P. Kruth, "Online quality control of selective laser melting," *22nd Annu. Int. Solid Free. Fabr. Symp. - Addit. Manuf. Conf. SFF 2011*, Jan. 2011.

[30] S. K. Everton, M. Hirsch, P. Stravroulakis, R. K. Leach, and A. T. Clare, "Review of in-situ process monitoring and in-situ metrology for metal additive manufacturing," *Mater. Des.*, vol. 95, pp. 431–445, Apr. 2016, doi: 10.1016/j.matdes.2016.01.099.

[31] M. Pavlov, M. Doubenskaia, and I. Smurov, "Pyrometric analysis of thermal processes in SLM technology," *Phys. Procedia*, vol. 5, pp. 523–531, Jan. 2010, doi: 10.1016/j.phpro.2010.08.080.

[32] "EOS GmbH," May 01, 2020. [Online]. Available: https://my.eos.info/#{1}

[33] "EOS GmbH." Oct. 15, 2021. [Online]. Available: https://learning.eos.info/ekp/servlet/ekp/login?target=%2Fekp%2Fservlet%2Fekp%2FpageLayout&TEMPLATE=&getnews=N&FAIL=Y&UID=bakir%40rti.zcu.cz&ERR=9